

New gravity-capillary waves at low speeds

Part 2: Nonlinear geometries

PHILIPPE H. TRINH^{1,2} AND S. JONATHAN CHAPMAN²

¹Program in Applied and Computational Mathematics, Princeton University,
Washington Road, Princeton, NJ, 08544, USA

²Oxford Centre for Industrial and Applied Mathematics, Mathematical Institute,
24-29 St. Giles', Oxford, Oxfordshire, OX1 3LB, UK

(Received — and in revised form —)

When traditional linearised theory is used to study gravity-capillary waves produced by flow past an obstruction, the geometry of the object is assumed to be small in one or several of its dimensions. In order to preserve the nonlinear nature of the obstruction, asymptotic expansions in the low-Froude or low-Bond number limits can be derived, but here, the solutions are waveless to every order. This is because the waves are in fact, exponentially small, and thus *beyond-all-orders* of regular asymptotics; their formation is a consequence of the divergence of the asymptotic series and the associated Stokes Phenomenon.

In Part 1, we showed how exponential asymptotics could be used to study the problem when the size of the obstruction is first linearised. In this paper, we extend the analysis to the nonlinear problem, thus allowing the full geometry to be considered at leading order. When applied to the classic problem of flow over a step, our analysis reveals the existence of six classes of gravity-capillary waves, from which two share a connection with the usual linearised solutions first discovered by Lord Rayleigh. The new solutions arise due to the availability of multiple singularities in the geometry, coupled with the interplay of gravitational and cohesive effects.

Key Words: surface gravity waves, capillary waves, wave-structure interactions

1. Introduction

Consider water that flows past a fishing line, which we model as a pressure distribution applied near the surface. As Lord Rayleigh (1883) demonstrated, if the velocity of the stream is kept above some critical velocity, then capillary waves are produced upstream and gravity waves downstream. However, if the speed of the stream is too small, then subcritical or supercritical solitary waves are produced instead. This classification of the dynamics holds similarly for many flows past more general obstructions, where we can linearise the geometry in one or several of its dimensions. Thus, typical linearised theory does not really distinguish between flows past differently shaped objects, but merely requires that they are sufficiently small [see *e.g.* Forbes (1983) and King & Bloor (1987)]. The question which we address in this paper is: *what can be said about gravity-capillary flows over obstructions which are not linearised?*

There are two important parameters: the Froude number, F (ratio of inertial to gravitational forces) and the Bond number, B (ratio of gravitational to surface tension forces). In

a previous work (Trinh & Chapman 2013*b*—henceforth referred to as Part 1) we showed how the typical linearised theory can be re-interpreted in the low-Froude and low-Bond limits. If q is the speed of the free-surface flow, and $F^2 = \mathcal{O}(\epsilon)$ while $B = \mathcal{O}(\epsilon^2)$, then the typical asymptotic expansion gives the *base series*, which we denote as $\textcircled{\text{B}}$, and write

$$\textcircled{\text{B}} \quad \left[q_0 + \epsilon q_1 + \epsilon^2 q_2 + \mathcal{O}(\epsilon^3) \right] e^0, \quad (1.1)$$

valid as $\epsilon \rightarrow 0$. The base series, $\textcircled{\text{B}}$, is waveless to every order, and in fact, the gravity and capillary waves are exponentially small and thus *beyond-all-orders*. These waves are *switched-on* when $\textcircled{\text{B}}$ is analytically continued across critical curves (*Stokes lines*) in the complex plane in a process known as the *Stokes Phenomenon*. We use the notation $\textcircled{\text{B}} > \textcircled{\text{G}}$ or $\textcircled{\text{B}} > \textcircled{\text{C}}$ to indicate the switching-on of a gravity or capillary wave, respectively, and these waves are written as

$$\textcircled{\text{G}} \quad \left[A_1 + \mathcal{O}(\epsilon) \right] e^{-\chi_g/\epsilon} \quad \text{and} \quad \textcircled{\text{C}} \quad \left[B_1 + \mathcal{O}(\epsilon) \right] e^{-\chi_c/\epsilon}. \quad (1.2)$$

In the linearised problem of flow over a step (Part 1), Stokes lines originate from the single, merged singularity which represents the step, and the point where the gravity and capillary waves are equal in magnitude corresponds to the critical bifurcation in the Froude-Bond plane.

The nonlinear analysis of this work differs from the linear analysis in two important ways. First, a nonlinear geometry usually contains multiple singularities and hence multiple Stokes lines; each singularity then has the potential to produce both gravity and capillary waves. Second, gravity and capillary waves can *themselves* interact, with $\textcircled{\text{G}} > \textcircled{\text{C}}$ or $\textcircled{\text{C}} > \textcircled{\text{G}}$. These more complicated secondary switchings may be accompanied by crossing Stokes lines, the higher-order Stokes Phenomenon, and other, more advanced, aspects of exponential asymptotics highlighted by Howls *et al.* (2004), Olde Daalhuis (2004), Chapman & Mortimer (2005), and Chapman *et al.* (2007).

Our main result shows that for a nonlinear obstruction, the typical bifurcation curve in the Froude-Bond plane *thickens*, revealing new possibilities for solutions. The thickness of this curve is a manifestation of the finite nature of the obstruction, and shrinks to zero as the geometry is linearised. For example, in the case of a rectangular step, rather than the two standard linear solutions of Lord Rayleigh (1883), there are now *six* possible solutions, for which the previous two are special cases.

1.1. Physical and mathematical background

A review of the physical and mathematical literature that motivates this work can be found in the introduction of Part 1 (Trinh & Chapman 2013*b*). The situation of free-surface gravity-capillary waves produced by flow past an obstruction is a well studied problem, and so we shall only mention the more comprehensive reviews of the topic by Dias & Kharif (1999) and Vanden-Broeck (2010), and of course, classic texts by Lamb (1932) and Stoker (1957).

As for the mathematical techniques we use in this paper known as *exponential asymptotics*, these are directly based on the methods introduced by Chapman *et al.* (1998) and previously applied to study wave-structure interactions for pure capillary waves (Chapman & Vanden-Broeck 2002), and pure gravity waves (Chapman & Vanden-Broeck 2006, Trinh *et al.* 2011, Lustri *et al.* 2012). A variety of other approaches to exponential asymptotics are available, and we refer the readers to the books by Dingle (1973), Costin (2008), and Boyd (1998) for an overview of the of the different techniques.

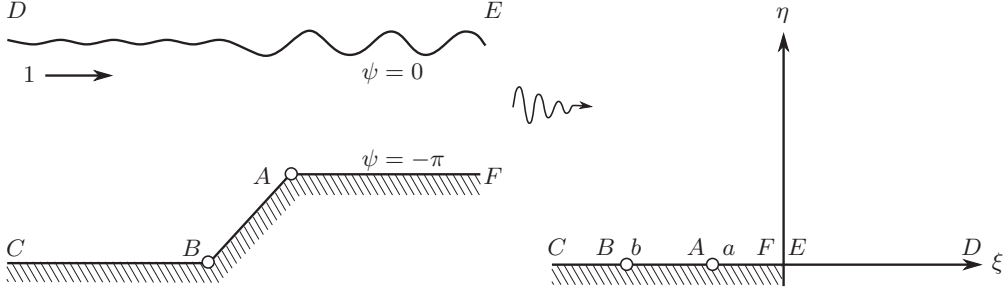


FIGURE 1. We consider a typical flow over an obstruction. The flow in the physical xy -plane (left) is first mapped to the potential $w = \phi + i\psi$ plane, then again mapped to the upper-half $\zeta = \xi + i\eta$ plane (right). For flow in a channel, the latter map is given by $\zeta = e^{-w}$.

2. Mathematical formulation

We briefly recapitulate the relevant equations, which parallel the ones presented in Part 1, but this time, we allow for the possibility of flows over more general geometries. Consider steady, two-dimensional potential flow of an incompressible fluid with upstream velocity U , and a prescribed length scale L . The flow is non-dimensionalised with characteristic scales of U and L/π for the velocity and lengths, respectively, and the physical $z = x + iy$ plane is mapped to the complex potential $w = \phi + i\psi$ plane, then mapped again to the upper-half $\zeta = \xi + i\eta$ plane using $\zeta = e^{-w}$. The free-surface is then given by

$$\log q = -\frac{1}{\pi} \int_{-\infty}^{\infty} \frac{\theta(\xi')}{\xi' - \xi} d\xi', \quad (2.1a)$$

$$\beta\epsilon \left[q^2 \frac{dq}{d\phi} \right] - \beta\tau\epsilon^2 \left[q^2 \frac{d^2\theta}{d\phi^2} + q \frac{dq}{d\phi} \frac{d\theta}{d\phi} \right] = -\sin \theta, \quad (2.1b)$$

where $F^2 = \beta\epsilon$ is the square of the Froude number, $B = \beta\tau\epsilon^2$ is the Bond number, and for hodograph variables $\log(dw/dz) = \log q - i\theta$, where q is the fluid speed and θ is the angle the streamlines make with the x -axis. This set-up is presented in Figure 1.

Our analysis must then be extended to the complexification of the free-surface (originally, q and θ for $\xi \in \mathbb{R}^+$). Complexifying the free-surface into the upper-half ξ -plane and relabeling $\xi \mapsto \zeta$ and $\phi \mapsto w$ gives

$$\log q - i\theta = -\frac{1}{\pi} \int_{-\infty}^0 \frac{\theta(\xi')}{\xi' - \zeta} d\xi' + \mathcal{H}\theta(\zeta), \quad (2.2a)$$

$$\beta\epsilon \left[q^2 \frac{dq}{dw} \right] - \beta\tau\epsilon^2 \left[q^2 \frac{d^2\theta}{dw^2} + q \frac{dq}{dw} \frac{d\theta}{dw} \right] = -\sin \theta. \quad (2.2b)$$

where \mathcal{H} denotes the Hilbert transform operator on the semi-infinite interval $\xi \geq 0$ which corresponds to the free-boundary, *i.e.*

$$\mathcal{H}\theta(\zeta) = -\frac{1}{\pi} \int_0^{\infty} \frac{\theta(\xi')}{\xi' - \zeta} d\xi'. \quad (2.3)$$

2.1. The inclined step

The methodology developed throughout this paper is applicable to most general non-surface-piercing geometries, which are chosen by imposing the value of θ along the negative $\zeta = \xi$ axis. With minimal modification, it can also be applied to surface-piercing obstructions (such as for a ship), the only significant difficulty being the assumptions-to-make near the point of contact [see Trinh *et al.* (2011)].

However, for concreteness and illustration, we will often take as an example the step in a channel, with

$$\zeta = e^{-w} \quad (2.4)$$

and

$$\theta = \begin{cases} 0 & \text{for } \zeta < -b \\ \sigma\pi & \text{for } \zeta \in (-b, -a) \\ 0 & \text{for } \zeta \in (-a, 0) \end{cases} \quad (2.5)$$

where $0 < a < b$. We will always imagine a stepping *up* (from left-to-right), with b associated with the stagnation point, a associated with the corner, and therefore $0 < \sigma < 1$. In the next section, we will see that at zero Froude and Bond numbers, the leading-order solution is provided by substituting the above values for θ along $\zeta < 0$, as well as $\theta = 0$ for $\zeta > 0$, into the boundary integral equation (2.2a), giving

$$q \sim \left(\frac{\zeta + b}{\zeta + a} \right)^\sigma \quad \text{and} \quad \theta = 0 + \mathcal{O}(\epsilon), \quad (2.6)$$

which is often termed the *rigid-wall flow*, as it is equivalent to replacing the free surface by the rigid wall, $\theta = 0$.

3. Asymptotic approximation

Substituting the usual perturbation expansions (the base series),

$$\theta \sim \sum_{n=0}^{\infty} \epsilon^n \theta_n \quad \text{and} \quad q \sim \sum_{n=0}^{\infty} \epsilon^n q_n \quad (3.1)$$

into (2.2a) and (2.2b) yields at $\mathcal{O}(1)$,

$$\theta_0 = 0, \quad (3.2a)$$

$$\log q_0 = -\frac{1}{\pi} \int_{-\infty}^0 \frac{\theta(\xi')}{\xi' - \zeta} d\xi', \quad (3.2b)$$

and at $\mathcal{O}(\epsilon)$,

$$q_0^2 \frac{dq_0}{dw} = -\frac{1}{\beta} \theta_1, \quad (3.2c)$$

$$\frac{q_1}{q_0} - i\theta_1 = \mathcal{H}\theta_1(\zeta). \quad (3.2d)$$

Notice that imposing the bottom topography in (3.2b) determines θ along $\xi \in \mathbb{R}^-$. The leading order solutions (3.2a)–(3.2b), simply correspond to the rigid wall flow whereby the free-surface is replaced by $\theta = 0$.

The full expressions for the higher $\mathcal{O}(\epsilon^n)$ terms are prohibitively complicated, but since we are mainly concerned with the limit $n \rightarrow \infty$, we may proceed in the following manner: the complexification of the leading-order free surface, q_0 will typically contain singularities, identifiable with singularities in the flow-domain, such as those corresponding to corners or stagnation points. However, because all the higher-order problems are linear, no new singularities can be introduced and thus, for all n , the singular points of q_n must be those *same* points as for q_0 .

Now if we examine the dynamic condition (2.2b), we can see that each successive term of the asymptotic approximation requires the derivative of the previous term. Then if q_n

contains a singularity of the form $1/(w - w^*)^n$, q_{n+1} will contain a singularity of the form $n/(w - w^*)^{n+1}$. Thus as $n \rightarrow \infty$, we can expect the late terms to behave like factorial over power, or

$$\theta_n \sim \frac{\Theta(w)\Gamma(n + \gamma)}{\chi(w)^{n+\gamma}} \quad \text{and} \quad q_n \sim \frac{Q(w)\Gamma(n + \gamma)}{\chi(w)^{n+\gamma}}. \quad (3.3)$$

In fact, the inductive argument used to explain the divergence of the asymptotic expansion according to (3.3) also serves to explain why the free surface waves are expected to be exponentially small in the limit $\epsilon \rightarrow 0$: the leading order solution (2.6) is waveless, and since the values of q_n and θ_n only depend on the derivatives of the previous orders, then none of the terms in the naive expansion (3.1) will contain waves.

Proceeding then with the ansatz (3.3), we can now pinpoint the necessary terms required at $\mathcal{O}(\epsilon^n)$. In the limit that $n \rightarrow \infty$, terms like $q_m q_n$ for m finite dominate terms with smaller indices in n , such as $q_m q_{n-1}$. Moreover, differentiating a term increases the order (in n) by 1, so a term like $\epsilon dq_{n-1}/dw$ is of the same order as q_n . The relevant terms at $\mathcal{O}(\epsilon^n)$ of the boundary integral equation (2.2a) are thus

$$\frac{q_n}{q_0} - \frac{q_{n-1}q_1}{q_0^2} + \dots - i\theta_n = \mathcal{H}\theta_n(\zeta),$$

for $n \geq 2$. It is known that as $n \rightarrow \infty$, the Hilbert transform on the right-hand side of this equation is exponentially subdominant to the terms on the left [see Part 1 or *e.g.* Chapman & Vanden-Broeck (2006) for further details]. Thus,

$$\theta_n \sim -i\frac{q_n}{q_0} + \frac{iq_1q_{n-1}}{q_0^2} + \dots \quad \text{as } n \rightarrow \infty, \quad (3.4)$$

or,

$$q_n \sim iq_0\theta_n + i\theta_{n-1}q_1 + \dots \quad \text{as } n \rightarrow \infty. \quad (3.5)$$

As for Bernoulli's Equation (2.2b), we will use (3.5) to replace q_n with θ_n , after which the relevant terms at $\mathcal{O}(\epsilon^n)$ are

$$\begin{aligned} & \overbrace{\left[iq_0^3 \theta'_{n-1} - [\tau q_0^2] \theta''_{n-2} + \left[\frac{1}{\beta} \right] \theta_n \right]}^{\text{first and second order as } n \rightarrow \infty} \\ & + \underbrace{\left[3iq_0^2 q'_0 \theta_{n-1} + [3iq_0^2 q_1 - \tau q_0 q'_0] \theta'_{n-2} - [2\tau q_0 q_1] \theta''_{n-3} \right]}_{\text{second order as } n \rightarrow \infty} = 0, \quad (3.6) \end{aligned}$$

with primes for differentiation in w . Using the ansatz (3.3) in the above equation, we have at leading order as $n \rightarrow \infty$,

$$-iq_0^3 \chi' - \tau q_0^2 (\chi')^2 + \frac{1}{\beta} = 0, \quad (3.7)$$

which is simply solved to give

$$\frac{d\chi}{dw} = -i \left[\frac{q_0^2 \pm \sqrt{\Delta}}{2\tau q_0} \right], \quad (3.8)$$

where

$$\Delta = q_0^4 - A \quad \text{and} \quad A = \frac{4\tau}{\beta}, \quad (3.9)$$

and A will turn out to be a key parameter. Remember that χ is the portion of the ansatz

(3.3) that expresses the singularities of the higher order terms. Since $\chi(w^*) = 0$ for one of these singularities, w^* , we may express

$$\chi_{\pm}(w) = -i \int_{w^*}^w \left[\frac{q_0^2 \pm \sqrt{\Delta}}{2\tau q_0} \right] d\varphi. \quad (3.10)$$

Note that in writing (3.10), we shall restrict the path of integration to be along *the same Riemann sheet* as w^* . Integration contours that traverse different sheets (for example, by crossing the branch cut(s) from $\Delta = 0$) will be addressed in later sections, and in particular, Appendix A. By taking the limit of (3.10) as $\tau \rightarrow 0$ and comparing with Chapman and Vanden-Broeck (2002; 2006), we see that the positive sign corresponds to capillary waves and the negative sign to gravity waves.

Now returning to the dynamic condition (3.6) and with the ansatzes (3.3), we find at next order in n :

$$\begin{aligned} & \left[iq_0^3 \right] \Theta' - \left[\tau q_0^2 \right] \left\{ -2\chi' \Theta' - \chi'' \Theta \right\} + \left[3iq_0^2 q_0' \right] \Theta \\ & + \left[3iq_0^2 q_1 - \tau q_0 q_0' \right] \left\{ -\chi' \Theta \right\} - \left[2\tau q_0 q_1 \right] \left\{ (\chi')^2 \Theta \right\} = 0. \end{aligned} \quad (3.11)$$

We may write this as

$$\frac{\Theta'}{\Theta} = -\frac{1}{4} \frac{\Delta'}{\Delta} \pm \frac{\Delta'}{2\sqrt{\Delta(\Delta+A)}} + F_{\pm}(w), \quad (3.12)$$

with

$$F_{\pm}(w) \equiv \frac{iq_1}{2\tau} \left[1 \pm \frac{\Delta + 2A}{\sqrt{\Delta(\Delta+A)}} \right], \quad (3.13)$$

and thus, after one integration,

$$\Theta(w) = \frac{(\sqrt{\Delta+A} + \sqrt{\Delta})^{\pm 1} \Lambda_{\pm}}{\Delta^{1/4}} \times \exp \left[\int_{w^{\star}}^w F_{\pm}(\varphi) d\varphi \right], \quad (3.14)$$

where Λ_{\pm} is a constant and we may begin the integration at any arbitrary point $w = w^{\star}$ where the integral is defined (often w^* is a natural choice for w^{\star} , but the integral may not exist at w^*). Note that (3.5), allows us to relate Q and Θ , with

$$Q \sim iq_0 \Theta. \quad (3.15)$$

As a check, we may take the limit of $\tau \rightarrow 0$ and use the negative sign of (3.14). This recovers the pre-factor for the gravity-wave problem,

$$\Theta_-(w) = -\frac{\Lambda_- i}{2q_0^3} \exp \left[-3i \int_{w^{\star}}^w \frac{q_1}{q_0^4} d\varphi \right], \quad (3.16)$$

to leading order, which differs from (3.16) in Chapman & Vanden-Broeck (2006) by a factor of a half (our Λ_- is their 2Λ).

A note on the \pm notation

As we have seen, each singularity is associated with two branches of $\chi = \chi_{\pm}$ in (3.10), for which the positive sign has been shown to correspond to capillary waves and the negative sign to gravity waves. There are also associated $\Theta = \Theta_{\pm}$, $Q = Q_{\pm}$, and $\Lambda = \Lambda_{\pm}$ quantities. In what follows, we will sometimes use non-subscripted variables if it is unimportant which branch of χ we are referring to.

4. Optimal truncation and Stokes line smoothing

The underlying divergence of the asymptotic expansions will cause the *Stokes Phenomenon* to occur: as the complexified asymptotic solution crosses a critical line (the *Stokes line*), a small exponential switches on. Because the switching-on of the exponential is almost always via an error function (Berry 1989), the optimal truncation and Stokes smoothing procedure will be similar to the one we performed in Part 1, with the exception of the nonlinear terms.

To begin, we *truncate* the asymptotic series at $n = \mathcal{N}$ so that

$$\theta = \sum_{n=0}^{\mathcal{N}-1} \epsilon^n \theta_n + R_{\mathcal{N}} \quad \text{and} \quad q = \sum_{n=0}^{\mathcal{N}-1} \epsilon^n q_n + S_{\mathcal{N}}, \quad (4.1)$$

where the remainders are related by (3.5) and thus

$$\frac{S_{\mathcal{N}}}{q_0} - \frac{\epsilon q_1 S_{\mathcal{N}}}{q_0^2} - \frac{\epsilon^{\mathcal{N}} q_1 q_{\mathcal{N}-1}}{q_0^2} + \dots = i R_{\mathcal{N}}. \quad (4.2)$$

We will substitute the truncated sums (4.1) into Bernoulli's Equation (2.2b) and in doing so, we will see two separate types of terms, the ones involving only q_n and θ_n , and the ones involving the remainders, $R_{\mathcal{N}}$ and $S_{\mathcal{N}}$.

Let us first study the terms involving the remainders. The remainder $S_{\mathcal{N}}$ can be written in terms of $R_{\mathcal{N}}$ by (4.2) and after making this substitution, we are particularly interested in the leading-order terms, which are indicated by factors of $R_{\mathcal{N}}$, $\epsilon R'_{\mathcal{N}}$, and $\epsilon^2 R''_{\mathcal{N}}$, and second-order terms, which are indicated by factors of $\epsilon R_{\mathcal{N}}$, $\epsilon^2 R'_{\mathcal{N}}$, and $\epsilon^3 R''_{\mathcal{N}}$. The relevant terms from Bernoulli's Equation are then given by the linear operator defined by

$$\begin{aligned} \mathcal{L}(R_{\mathcal{N}}; \epsilon) = & \left[i q_0^3 \right] \epsilon R'_{\mathcal{N}} - \left[\tau q_0^2 \right] \epsilon^2 R''_{\mathcal{N}} + \left[\frac{1}{\beta} \right] R_{\mathcal{N}} \\ & + \left[3 i q_0^2 q'_0 \right] \epsilon R_{\mathcal{N}} + \left[3 i q_0^2 q_1 - \tau q_0 q'_0 \right] \epsilon^2 R'_{\mathcal{N}} - \left[2 \tau q_0 q_1 \right] \epsilon^3 R''_{\mathcal{N}}, \end{aligned} \quad (4.3)$$

which is exactly the same form as the left of (3.6). We then introduce the Stokes smoothing parameter, $\mathcal{S} = \mathcal{S}(w)$, and set $R_{\mathcal{N}} = \mathcal{S}[\Theta e^{-\chi/\epsilon}]$. We know that the ansatz $\Theta e^{-\chi/\epsilon}$ solves $\mathcal{L} = 0$, so only terms involving derivatives of \mathcal{S} will be left. After some computation, we find to leading order,

$$\mathcal{L}(R_{\mathcal{N}}; \epsilon) \sim \epsilon \Theta e^{-\chi/\epsilon} \frac{d\mathcal{S}}{dw} \left[i q_0^3 + 2 \tau q_0^2 \chi' \right].$$

Writing $d\mathcal{S}/dw = \chi' d\mathcal{S}/d\chi$, and using (3.7) gives

$$\mathcal{L}(R_{\mathcal{N}}; \epsilon) \sim \epsilon \Theta e^{-\chi/\epsilon} \frac{d\mathcal{S}}{d\chi} \left[\frac{1}{\beta} + \tau q_0^2 (\chi')^2 \right].$$

Now let us turn to the terms involving q_n and θ_n : when the truncated sum in (4.1) is substituted into (2.2b), terms of $\mathcal{O}(\epsilon^{\mathcal{N}-1})$ will automatically be satisfied, and this process leaves us only with the remnant $\mathcal{O}(\epsilon^{\mathcal{N}})$ contributions from the inertial terms, as well as the $\mathcal{O}(\epsilon^{\mathcal{N}})$ and $\mathcal{O}(\epsilon^{\mathcal{N}+1})$ contributions from the surface-tension terms:

$$\begin{aligned} \epsilon^{\mathcal{N}} \left[q_0^2 \frac{dq_{\mathcal{N}-1}}{dw} + \dots \right] - \epsilon^{\mathcal{N}} \tau \left[q_0^2 \frac{d^2 \theta_{\mathcal{N}-2}}{dw^2} + \dots \right] - \epsilon^{\mathcal{N}+1} \tau \left[q_0^2 \frac{d^2 \theta_{\mathcal{N}-1}}{dw^2} + \dots \right] \\ = \epsilon^{\mathcal{N}} \left[-\frac{\theta_{\mathcal{N}}}{\beta} + \dots \right] - \epsilon^{\mathcal{N}+1} \tau \left[q_0^2 \frac{d^2 \theta_{\mathcal{N}-1}}{dw^2} + \dots \right], \end{aligned} \quad (4.4)$$

and thus in total we have

$$\mathcal{L}(R_{\mathcal{N}}; \epsilon) \sim \epsilon^{\mathcal{N}} \left[\frac{\theta_{\mathcal{N}}}{\beta} + \epsilon \tau q_0^2 \frac{d^2 \theta_{\mathcal{N}-1}}{dw^2} \right]. \quad (4.5)$$

Since we are interested in the limit $\epsilon \rightarrow 0$ when $\mathcal{N} \rightarrow \infty$, we can substitute the late-orders ansatz of (3.3) into the right-hand side of (4.5), giving

$$\mathcal{L}(R_{\mathcal{N}}; \epsilon) \sim \frac{\epsilon^{\mathcal{N}} \Theta \Gamma(\mathcal{N} + \gamma)}{\chi^{\mathcal{N} + \gamma}} \left[\frac{1}{\beta} + \tau q_0^2 (\chi')^2 \frac{\epsilon(\mathcal{N} + \gamma + 1)}{\chi} \right]. \quad (4.6)$$

We introduce a coordinate system along the Stokes line using $\chi = r e^{i\vartheta}$. The optimal truncation point (where adjacent terms of the expansion are equal in size) is at $[r/\epsilon]$, so we write $\mathcal{N} = r/\epsilon + \rho$ where $\rho \in [0, 1)$. Changing to differentiation in ϑ , using

$$\frac{d}{d\chi} = -i \frac{e^{-i\vartheta}}{r} \frac{d}{d\vartheta},$$

and applying Stirling's formula to (4.6) gives

$$\frac{d\mathcal{S}}{d\vartheta} \left[\frac{1}{\beta} + \tau q_0^2 (\chi')^2 \right] \sim \frac{\sqrt{2\pi r}}{\epsilon^{\gamma+1/2}} \left[\frac{1}{\beta} + \frac{\tau q_0^2 (\chi')^2}{e^{i\vartheta}} \right] (e^{-i\vartheta})^{r/\epsilon + \rho + \gamma} e^{r e^{i\vartheta}/\epsilon} e^{-r/\epsilon}.$$

The exponential factor on the right is exponentially small, except near the Stokes line $\vartheta = 0$, where the critical scaling occurs with $\vartheta = \sqrt{\epsilon \bar{\vartheta}}$. In total, then,

$$\frac{d\mathcal{S}}{d\bar{\vartheta}} \sim \frac{i\sqrt{2\pi r}}{\epsilon^\gamma} \exp\left(-\frac{r\bar{\vartheta}^2}{2}\right),$$

and we have recovered the typical error function expression for the Stokes multiplier, \mathcal{S} . We now integrate this expression across the Stokes line from upstream, or $\bar{\vartheta} = \infty$, to downstream, or $\bar{\vartheta} = -\infty$. The apparent jump in the remainders of θ and q are then

$$\left[R_{\mathcal{N}} \right]_{\text{upstream}}^{\text{downstream}} \sim -\frac{2\pi i}{\epsilon^\gamma} \Theta e^{-\chi/\epsilon} \equiv \theta_{\text{exp}}, \quad (4.7a)$$

$$\left[S_{\mathcal{N}} \right]_{\text{upstream}}^{\text{downstream}} \sim -\frac{2\pi i}{\epsilon^\gamma} Q e^{-\chi/\epsilon} \equiv q_{\text{exp}} \quad (4.7b)$$

We can re-introduce the notation for the switching-on mechanism used in Part 1. We write, for example,

$$\sum_n \epsilon^n q_n \xrightarrow{\text{Stag.} \atop \textcircled{\text{B}} > \textcircled{\text{C}}} \sum_n \epsilon^n q_n + q_{\text{exp}}$$

$$\sum_n \epsilon^n q_n \xrightarrow{\text{Corn.} \atop \textcircled{\text{B}} > \textcircled{\text{G}}} \sum_n \epsilon^n q_n + q_{\text{exp}},$$

and the arrow notation should be read as ‘‘the base series turns on a capillary/gravity wave as the Stokes line from the stagnation/corner point is crossed’’.

To finalise the analysis, we need to also complexify the free boundary into the lower-half plane. This analogous process yields the functional complex conjugates of (4.7a) and (4.7b), and thus the total leading order contribution along the free-surface is given by twice the real parts of (4.7a) and (4.7b),

$$q_{\text{exp, total}} \sim -\frac{4\pi}{\epsilon^\gamma} \Im \left(Q e^{-\chi/\epsilon} \right), \quad (4.8a)$$

$$\theta_{\text{exp, total}} \sim -\frac{4\pi}{\epsilon^\gamma} \Im \left(\Theta e^{-\chi/\epsilon} \right). \quad (4.8b)$$

In order to fully determine the waves, we must also compute the values of the prefactor, Λ , that appears in (3.15) and (3.16) for Q and Θ , and also the value of γ in (4.8). This can be done by matching the outer solution (3.1) with an inner solution valid near each of the singularities. Although this was easily done for the linear problem in Part 1, the nonlinear problem is much more tedious, and readers can refer to Trinh (2010) for the detailed procedure.

5. Inner limits of χ and Stokes lines

In the low-Froude and low-Bond limits, we can think of the exponentially small free-surface waves as having been generated by singularities in the flow domain. For example, in the case of the step (2.6), both the corner and stagnation points are responsible for producing waves through their associated Stokes lines. Furthermore, we know from Dingle (1973) that Stokes lines with $\textcircled{B} > \textcircled{C}$ or $\textcircled{B} > \textcircled{D}$, are given at points where the base series (with phase zero) reaches peak exponential dominance over the capillary or gravity waves (with phase $-\chi/\epsilon$). This yields the two conditions

$$\Im(\chi_{\pm}) = 0 \quad \text{and} \quad \Re(\chi_{\pm}) \geq 0, \quad (5.1)$$

and for a given geometry, the trajectory of the Stokes lines can be derived by numerically evaluating the integral (3.10) and applying conditions (5.1). Whether a Stokes line encounters the free surface is a problem that thus depends on the global behaviour of q_0 ; however, we can still study the local properties of the Stokes lines near their associated singularities.

5.1. Local Stokes line analysis for general channel flows

Let us assume that there is a singularity in the outer solutions (3.1) at the points $z = z^*$, $w = w^*$, and $\zeta = \zeta^*$, which correspond to the different planes introduced in Figure 1. We introduce the shifted coordinate $W = w - w^*$, and then from potential theory, $W \sim \text{const} \times (z - z^*)^{\kappa}$ for some κ ; in the case of stagnation points, $\kappa = 2$, while for corner singularities, $\kappa = \pi/\nu$, where ν is the in-fluid angle of the corner. In the analytic continuation of the free boundary, we have from the definition of the complex velocity,

$$\frac{dw}{dz} \sim q_0 e^{-i\theta_0} = q_0 = \text{const} \times (z - z^*)^{\kappa-1} = \text{const} \times W^{(\kappa-1)/\kappa}, \quad (5.2)$$

and thus the inner limit of the outer solution is given by

$$q \sim c(w - w^*)^{\alpha} = cW^{\alpha} \quad (5.3)$$

where $\alpha = (\kappa - 1)/\kappa$ and c is constant.

Using χ in (3.8) and the limiting form for q_0 in (5.3), we see that χ must exhibit different limiting behaviours as the singularity is approached, depending on which sign of the square root is chosen and whether α is positive or negative:

$$\chi_{\pm} \sim \begin{cases} \left[-\frac{ic}{\tau(\alpha+1)} \right] W^{\alpha+1} & \equiv X_3 W^{\alpha+1} & \text{for capillary (+) and } \alpha < 0 \\ \left[-\frac{i}{c^3\beta(1-3\alpha)} \right] W^{1-3\alpha} & \equiv X_2 W^{1-3\alpha} & \text{for gravity (-) and } \alpha < 0 \\ \left[\mp \frac{ie^{\text{Arg}(\Delta)/2}}{c\sqrt{\beta\tau}(1-\alpha)} \right] W^{1-\alpha} & \equiv X_1^{\pm} W^{1-\alpha} & \text{for } \alpha > 0 \end{cases} \quad (5.4)$$

For $\alpha < 0$, the choice of the negative sign for the square root leads to gravity waves,

whereas the positive sign is associated with capillary waves; this is clear from the appearance of either β (gravity) or τ (capillary) in the coefficients of χ , but can also be understood by taking $\tau \rightarrow 0$, and noticing that the capillary root in (3.7) disappears to infinity, leaving only the gravity root.

There is a notable difficulty in determining the local behaviour of χ_{\pm} in (5.4) when $\alpha > 0$, and this deals with the value of $\text{Arg}(\Delta)$, which must tend to π or $-\pi$ as we approach the singularity from the upper half- ζ -plane. For the purpose of the Stokes line analysis in the next section, it is sufficient to see that if we approach the singularity from along the upstream boundary, and set $W = |W|e^{i\pi}$, then $\Im(q_0^4 - A)$ tends to zero from below as $|W| \rightarrow 0$, and thus

$$e^{\text{Arg}(\Delta)/2} = -i. \quad (5.5)$$

We also mention that the assumption that the potential follows a power of $(z - z^*)$ in (5.2) will not be true for the case of a sink or source, where $W \sim \text{const.} \times \log(z - z^*)$. However, this analysis requires a somewhat different approach because the location of the singularity corresponds to $|w| \rightarrow \infty$. The problem of applying exponential asymptotics to gravity flow past a submerged line source was studied by Lustri *et al.* (2013).

5.2. Local Stokes line analysis for the step

The existence of a Stokes line does not necessarily guarantee the appearance of surface waves. Indeed there are cases where the associated Stokes line fails to intersect the free-surface, as well as cases where the line lies on a different Riemann sheet altogether. In this section, we study the simplest scenario of a Stokes line which emerges from its singularity in the ‘in-fluid’ direction of the upper-half ζ -plane. Whether such a line actually encounters the free-surface ($\zeta \in \mathbb{R}^+$) is a global function of the leading-order flow and in general, must be checked by evaluating the integral in (3.10). For the moment, we ignore lines which leave in a direction of ‘into’ the boundary ($\Im(\zeta) < 0$), and lines which enter secondary Riemann sheets. From a study of the global contours of χ , we have observed that relevant interactions are generally governed by Stokes lines that traverse simple paths (from singularity to free-surface along the same Riemann sheet). However, in §7 and Appendix A, we shall see the role played by more complicated Stokes line trajectories which cross onto different sheets.

Recall that the value of α in (5.3) determines the boundary’s geometry near the singularity, with $\alpha < 0$ for a corner and $\alpha > 0$ for a stagnation point. The value of c determines the orientation of the geometry, and this is not quite arbitrary because gravity provides a reference direction. Again, let us consider the two singularities associated with the step geometry in (2.6).

For the case of the corner, with $\alpha \in (-1, 0)$ and $c \in \mathbb{R}^+$, then in the notation of (5.4),

$$\chi_{\pm} \sim \begin{cases} |X_3|e^{-\pi i/2}W^{\alpha+1} & \text{for capillary (+)} \\ |X_2|e^{-\pi i/2}W^{1-3\alpha} & \text{for gravity (-)} \end{cases} \quad (5.6)$$

as $W \rightarrow 0$. If we write $\vartheta_{\text{grav}} = \text{Arg}(W)$ for the local angle of a gravity Stokes line, and ϑ_{cap} for the local angle of a capillary Stokes line, then we have from (5.1) that

$$\vartheta_{\text{grav}} = \pi \left(\frac{2m + 1/2}{1 - 3\alpha} \right) \quad \text{and} \quad \vartheta_{\text{cap}} = \pi \left(\frac{2m + 1/2}{\alpha + 1} \right),$$

where $m \in \mathbb{Z}$. As α increases from -1 to 0 , the first ($m = 0$) gravity Stokes line increases from $\vartheta_{\text{grav}} = \pi/8$ to $\pi/2$. However, for the same range in α , the first capillary Stokes line only enters the upper-half plane beginning at $\alpha = -1/2$, where $\vartheta_{\text{cap}} = \pi$. As α increases to 0 , ϑ_{cap} increases to $\pi/2$. By taking the local analysis to next order in W , it can be

shown in the case of the Stokes line initially leaving along the boundary, $\vartheta_{\text{cap}} = \pi$, it must continue along the boundary until it encounters the stagnation point.

For the case of the stagnation point, with $\alpha \in (0, 1)$ and $c = |c|e^{-\pi i\alpha}$, then (5.4) gives

$$\chi_{\pm} \sim \mp |X_1| e^{\pi i\alpha} W^{1-\alpha},$$

as $W \rightarrow 0$ once we have used (5.5). The Stokes lines leave at angles of

$$\vartheta_{\text{grav}} = \pi \left(\frac{2m - \alpha}{1 - \alpha} \right) \quad \text{and} \quad \vartheta_{\text{cap}} = \pi \left(\frac{2m - 1 - \alpha}{1 - \alpha} \right),$$

for $m \in \mathbb{Z}$. For gravity waves, there are no relevant Stokes lines lying in the upper half-plane. For capillary waves, the only relevant value of m is 1, which shows that there exists a Stokes line along $\theta = \pi$ for all shapes. However, a secondary analysis to next order in W shows that the Stokes line which initially tends along $\vartheta_{\text{cap}} = \pi$ does indeed leave the boundary into the upper half-plane.

The local Stokes line angles in the physical plane can be retrieved by using (5.2) and (5.3). If $z = z^*$ is the corresponding singularity, then

$$z - z^* \sim \left[\frac{1}{c(1 - \alpha)} \right] W^{1-\alpha}. \quad (5.7)$$

In summary, given a step-up obstruction with initial inclination $\sigma\pi$, the following occurs: first, the stagnation point always produces a capillary Stokes line; second, the corner always produces a gravity Stokes line, and only produces a capillary Stokes line if $\sigma > 1/2$. Table 1 provides an illustration of our local Stokes line analysis. Note that at $\alpha = 0$, there is no singularity, so the corresponding entry instead refers to the limiting process of $\alpha \rightarrow 0^-$.

6. Turning points and Stokes lines for the step

The singularities encountered in §5 are not the only critical points in the gravity-capillary problem. From (3.9), the *turning points*, $\zeta = \zeta_T$, found at

$$\Delta = q_0^4 - A = q_0^4 - \frac{4\tau}{\beta} = 0, \quad (6.1)$$

also represent a type of wave-generating singularity. These points do not share a connection with the physical geometry, but rather, they correspond to locations where derivatives of the capillary and gravity wavenumbers are equal. By drawing an analogy to the Airy equation (White 2005, Chap. 11), we would expect that these turning points can also produce Stokes lines, across which gravity and capillary waves can themselves interact.

Care must be taken in solving $\Delta = 0$, however, since this generally involves the inversion of composite complex-valued functions with multiple branch cuts. In the case of the step flow (2.6), for example, since $A > 0$, all the possible solutions are given by

$$\left(\frac{\zeta_T + b}{\zeta_T + a} \right) = A^{1/4\sigma} e^{2\pi i k / 4\sigma}. \quad (6.2)$$

Different values of $k \in \mathbb{Z}$ in (6.2) may correspond to different turning points, but we must always check (*a posteriori*) that the final location lies on the main Riemann sheet (*i.e.* where q_0 is real and positive on $\zeta \in \mathbb{R}^+$). Like the previous Stokes line analysis of §5.2, we only consider points on this immediate sheet; numerical computations of the global

Local power (α)	Grav. Stokes (ϑ_{grav})	Cap. Stokes (ϑ_{cap})	Physical sketch
-1	$\frac{\pi}{8}$	none	
$(-1, -\frac{1}{2})$	$(\frac{\pi}{8}, \frac{\pi}{5})$	none	
$-\frac{1}{2}$	$\frac{\pi}{5}$	π	
$(-\frac{1}{2}, 0)$	$(\frac{\pi}{5}, \frac{\pi}{2})$	$(\pi, \frac{\pi}{2})$	
0	$\frac{\pi}{2}$	$\frac{\pi}{2}$	
$(0, 1)$	none	π	

TABLE 1. A summary of the local behaviour of a Stokes line (shown dashed) as it emerges from a singularity for which the complex velocity behaves like $dw/dz \sim c(w - w^*)^\alpha$. Angles ϑ are relative to the positive $\Re(w)$ -axis. Angles in the physical plane follow from (5.7) and the solid arrow indicates the direction of flow.

contours of χ seem to indicate that critical points that lie on secondary sheets do not affect the free surface (though there are exceptions: see Appendix A).

There are three important turning points in (6.2), which we denote as $\zeta_T = \zeta_1, \zeta_2$, and ζ_3 , corresponding to $k = 0, 1$, and -1 , respectively. Their locations for various values of σ and A are shown in the main portion of Figure 2. Recall that the upper half- ζ -plane shares a connection with the z -plane, and we have illustrated the physical connection within the insets (a) to (f). Note that we have taken the branch cut, marked by a striped line, along the real axis in the ζ -plane, between the corner and stagnation points.

First consider the two complex turning points, ζ_2 and ζ_3 . For a fixed values of A and $\sigma > 0.5$, the point ζ_2 lies somewhere above the real axis, and ζ_3 is its conjugate. For fixed σ and as $A \rightarrow 0$, ζ_2 tends to the stagnation point, while if $A \rightarrow \infty$, ζ_2 tends to the corner point. This motion for variable A is shown as a solid curve in Figure 2. On the other hand, if A is fixed and $\sigma \rightarrow 0.5$, ζ_2 moves towards the branch cut, so that at $\sigma = 0.5$, ζ_2 lies directly on the angled step, while ζ_3 has moved onto the adjacent Riemann sheet. If

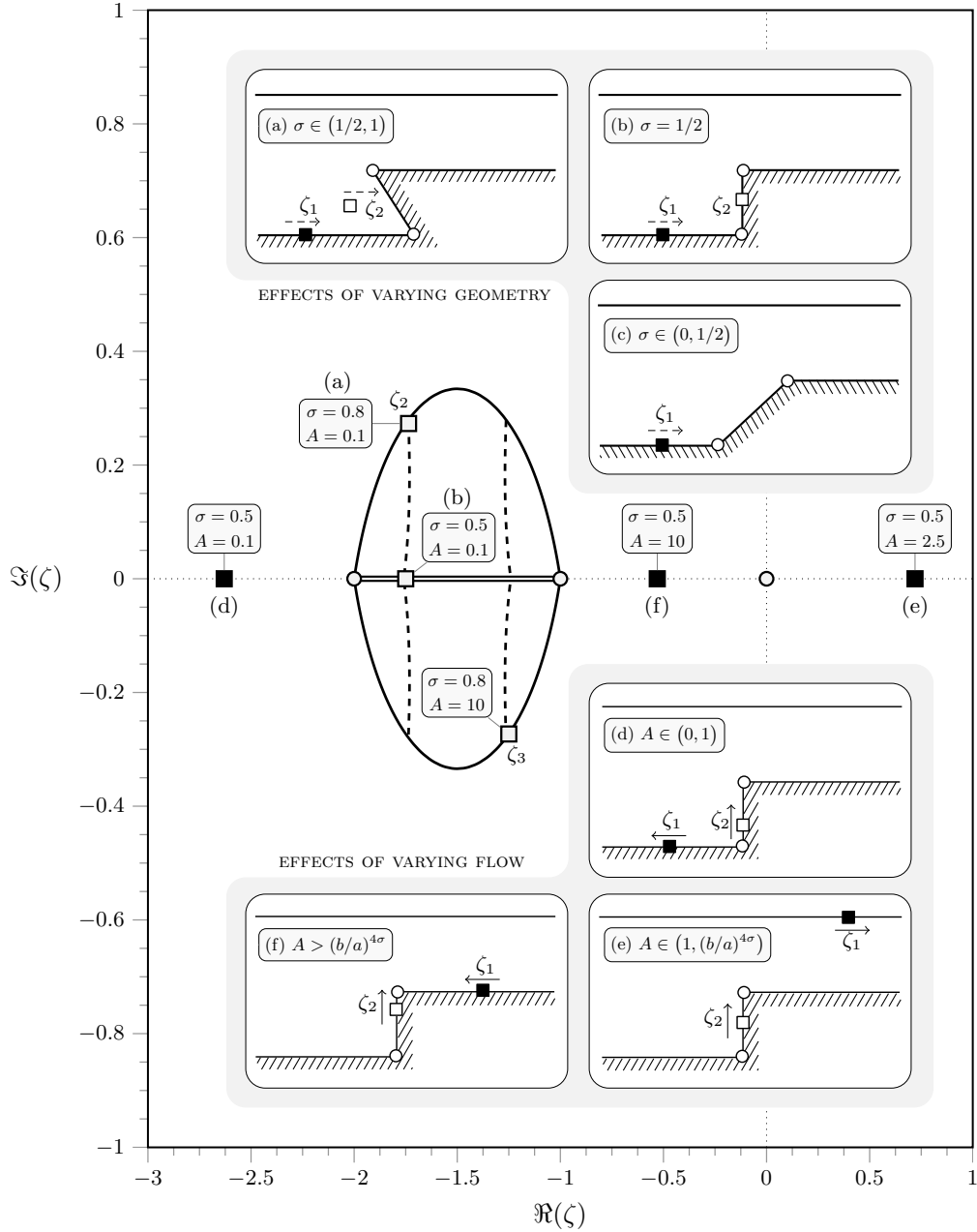


FIGURE 2. Movement of the turning points, ζ_1 , ζ_2 , ζ_3 for the step with $b = 2$ (stagnation point) and $a = 1$ (corner). Exact values are shown in the ζ -plane and the insets provide depictions in the physical plane. The ζ_1 points are black squares, and $\zeta_{2,3}$ are grey squares. For fixed values of A and decreasing values of σ (thus fixing the flow parameters, but changing the geometry), the different values of ζ_2 and ζ_3 are shown as a dashed line in the main illustration and through insets (a) to (c). Similarly, for changing values of A and fixed values of σ (thus changing the flow parameters, but fixing the geometry), the values of $\zeta_{2,3}$ are shown as a solid line in the main illustration, and through insets (d)–(f). Note that for $\sigma < 0.5$, both ζ_2 and ζ_3 have passed over to the adjacent Riemann sheets, so they have disappeared from the physical illustration (c).

$\sigma < 0.5$, then both ζ_1 and ζ_3 are now on secondary sheets. This motion for variable σ is shown as the dashed line in the figure, and through the insets (a) to (c).

The turning point, $\zeta_T = \zeta_1$, is real for all values of σ and A . When $A = 0$, ζ_1 lies on top of the stagnation point, and as $A \rightarrow \infty$, ζ_1 moves leftwards along the real ζ -axis towards the corner point by passing through $|\zeta| = \infty$ and traversing the free-surface. There are two special points: $A = 1$ (when ζ_1 has reached infinity upstream), and $A = (b/a)^{4\sigma}$ (when ζ_1 has reached infinity downstream). This is illustrated for the case of a rectangular step in Figure 2, and insets (d) to (f).

6.1. Inner analysis and reduction to the Airy Equation

Turning points are important for two reasons: first, a turning point which lies on the free surface, as in the case of $A > 1$, produces a change in one or both gravity and capillary waves from constant-amplitude oscillations to exponential decay [c.f. $\Re(d\chi/dw)$ in (3.8)]; second, turning points also generate Stokes lines and can thus lead to the birth of new exponentials. Recall from (4.7b) that, upon crossing the $\textcircled{B} > \textcircled{G}$ or $\textcircled{B} > \textcircled{C}$ Stokes line from $\zeta = \zeta^*$, the base series switches on the exponential

$$q_{\text{exp}} = -\frac{2\pi i Q_{\pm}(\zeta)}{\epsilon^\gamma} \exp\left[-\frac{1}{\epsilon} \int_{\zeta^*}^{\zeta_T} \frac{d\chi_{\pm}}{d\zeta'} d\zeta'\right] \exp\left[-\frac{1}{\epsilon} \int_{\zeta_T}^{\zeta} \frac{d\chi_{\pm}}{d\zeta'} d\zeta'\right], \quad (6.3)$$

which we have written so that the integration passes through an arbitrary turning point, $\zeta = \zeta_T$. The Stokes lines from the turning points are given at locations where one exponential (e.g. gravity) reaches peak exponential dominance over the other (e.g. capillary). Thus,

$$\begin{aligned} \textcircled{G} > \textcircled{C} : \quad \Re\left[-\int_{\zeta_T}^{\zeta} \frac{d\chi_-}{d\zeta'} d\zeta'\right] &\geq \Re\left[-\int_{\zeta_T}^{\zeta} \frac{d\chi_+}{d\zeta'} d\zeta'\right], \\ \textcircled{C} > \textcircled{G} : \quad \Re\left[-\int_{\zeta_T}^{\zeta} \frac{d\chi_+}{d\zeta'} d\zeta'\right] &\geq \Re\left[-\int_{\zeta_T}^{\zeta} \frac{d\chi_-}{d\zeta'} d\zeta'\right]. \end{aligned} \quad (6.4)$$

As $\zeta \rightarrow \zeta_T$, it is easy to verify from (6.2) that the turning points are *simple*, and so we may write

$$\Delta \sim D(\zeta - \zeta_T), \quad (6.5)$$

where $D \in \mathbb{C}$. Also, from (3.14) and (3.15), we have that

$$Q_{\pm} \sim \frac{B_{\pm}}{(\zeta - \zeta_T)^{1/4}} \quad (6.6)$$

where B_{\pm} is constant. We now write (6.3) in a form that makes the connection to the Airy equation apparent. We introduce

$$H_{\pm}(\zeta) \equiv -\frac{2\pi i}{\epsilon^\gamma} (\zeta - \zeta_T)^{1/4} Q_{\pm} \exp\left[-\frac{1}{\epsilon} \int_{\zeta^*}^{\zeta_T} \frac{d\chi_{\pm}}{d\zeta'} d\zeta'\right], \quad (6.7)$$

so H_{\pm} tends to a constant near the turning points. We also split the real and complex parts of χ in (3.10) with $d\chi_{\pm}/d\zeta = (S_1 \pm iS_2)$, where

$$S_1(\zeta) = -(dw/d\zeta) \frac{i q_0}{2\tau} \quad \text{and} \quad S_2(\zeta) = -(dw/d\zeta) \frac{\sqrt{\Delta}}{2\tau q_0} \quad (6.8)$$

and $dw/d\zeta = -1/\zeta$ is given by (2.4) for the particular case of a channel geometry. The

expression for q_{exp} in (6.3) can now be written as

$$q_{\text{exp}} = \left[H_{\pm} \exp \left(-\frac{1}{\epsilon} \int_{\zeta_T}^{\zeta} S_1 d\zeta' \right) \right] \times \frac{\exp \left(\mp \frac{i}{\epsilon} \int_{\zeta_T}^{\zeta} S_2 d\zeta' \right)}{(\zeta - \zeta_T)^{1/4}}, \quad (6.9)$$

Following the discussion of §6, we shall assume that $\zeta = \zeta_T$ is a first-order turning point (although this may not be true of all possible geometries specified by q_0). If we like, we can re-scale q and ζ near $\zeta = \zeta_T$ in order to remove the square-bracketed pre-factor of (6.9). The governing equations (2.2a)–(2.2b) would then reduce to an Airy equation (*c.f.* Bender & Orszag 1978), for which we can perform the local Stokes line analysis. However, it is faster to apply the following shortcut: using the local expression for Δ in (6.5), and combining with (6.7)–(6.9) gives

$$q_{\text{exp}} \sim H_{\pm}(\zeta_T) \frac{e^{\mp \frac{p}{\epsilon}(\zeta - \zeta_T)^{3/2}}}{(\zeta - \zeta_T)^{1/4}}, \quad (6.10)$$

valid in the limit $\zeta \rightarrow \zeta_T$, where $p \in \mathbb{C}$ is a constant that depends on ζ_T .

We then note that the Airy switching requires

$$\frac{e^{\mp \frac{p}{\epsilon}(\zeta - \zeta_T)^{3/2}}}{(\zeta - \zeta_T)^{1/4}} \xrightarrow[\textcircled{\cong}]{\text{Turning Point}} \frac{e^{\mp \frac{p}{\epsilon}(\zeta - \zeta_T)^{3/2}}}{(\zeta - \zeta_T)^{1/4}} + iM \frac{e^{\pm \frac{p}{\epsilon}(\zeta - \zeta_T)^{3/2}}}{(\zeta - \zeta_T)^{1/4}}, \quad (6.11)$$

that is, the dominant wave switches on the subdominant wave with a Stokes multiplier of i (White 2005, Chap. 11). The quantity $M = \pm 1$ inserts a sign that depends on the direction of analytic continuation past the Stokes line (the standard Airy equation, for example, has $M = 1$ for analytic continuation in the counter-clockwise direction, relative to the turning point).

In terms of the outer variables, q , this shows that as we analytically continue across a Stokes line from the turning point at $\zeta = \zeta_T$, the already existent capillary/gravity wave in (6.3)

$$q_{\text{exp}} = \left[-\frac{2\pi i Q_{\pm}}{\epsilon^{\gamma}} \right] \times \exp \left[-\frac{1}{\epsilon} \int_{\zeta^*}^{\zeta} \frac{d\chi_{\pm}}{d\zeta'} d\zeta' \right], \quad (6.12)$$

switches on a gravity/capillary wave, which satisfies the transition rule:

$$q_{\text{exp}} \xrightarrow[\textcircled{\cong}]{\text{Turning Point}} q_{\text{exp}} + iM \left[-\frac{2\pi i Q_{\mp}}{\epsilon^{\gamma}} \right] \left[\frac{B_{\pm}}{B_{\mp}} \right] \\ \times \exp \left[-\frac{1}{\epsilon} \left(\int_{\zeta^*}^{\zeta_T} \frac{d\chi_{\pm}}{d\zeta'} d\zeta' + \int_{\zeta_T}^{\zeta^*} \frac{d\chi_{\mp}}{d\zeta'} d\zeta' \right) \right] \times \exp \left[-\frac{1}{\epsilon} \int_{\zeta^*}^{\zeta} \frac{d\chi_{\mp}}{d\zeta'} d\zeta' \right], \quad (6.13)$$

where B_{\pm} is given by (6.6). We have written the integrals in (6.13) so as to emphasise the turning-point process. Notice that the last exponential in (6.13) clearly indicates the presence of a gravity/capillary wave [(6.12) with a negated exponential]. The first two integrals of (6.13), however, show that the original capillary/gravity wave was generated from ζ^* on the \pm branch, went around the turning point ζ_T , and returned to ζ^* along the \mp branch. The values of most of the quantities (*e.g.* Q_{\pm} , B_{\pm} , and M) will not be necessary for the following discussion, but can be numerically computed if required.

7. New solutions for the rectangular step ($\sigma = 1/2$)

In the spirit of King & Bloor (1987) and Chapman & Vanden-Broeck (2006), we now study the simplest case for a non-trivial step: the rectangular geometry. In Part 1 of our

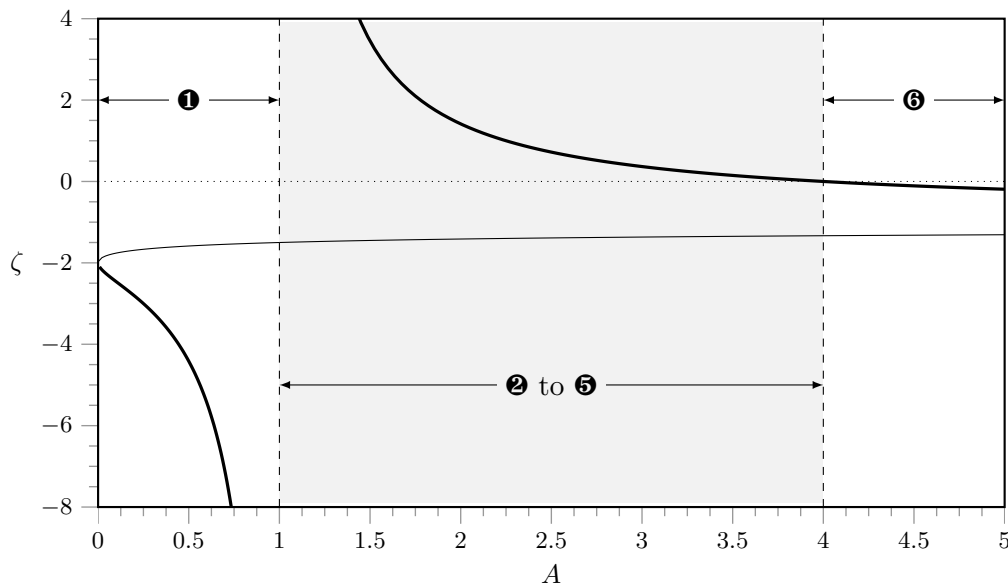


FIGURE 3. Positions of the two turning points (7.1) as a function of $A = 4\tau/\beta$ for the case of a rectangular step with $a = 1$ and $b = 2$. The T_1 turning point at $\zeta = \zeta_1$ is shown thick, and the T_2 turning point at $\zeta = \zeta_2$ is shown thin.

work, it was shown that for the case of a linearised step of small height, two solutions are possible at small Froude and Bond numbers: one with capillary waves upstream and gravity waves downstream, and the other with localised solitary waves with decaying oscillations in the far field. Furthermore, this bifurcation arises because the capillary and gravity Stokes lines coalesce.

However, for the nonlinear step, there is the added subtlety in the form of the turning points. As we know from §6, turning points not only change constant-amplitude waves to exponential decay, but also switch on secondary gravity or capillary waves. For the rectangular step, the two turning points are given by (6.2), simplified to

$$\zeta_1 = \frac{-b + a\sqrt{A}}{1 - \sqrt{A}} \quad \text{and} \quad \zeta_2 = \frac{-b - a\sqrt{A}}{1 + \sqrt{A}}, \quad (7.1)$$

and these are shown in Figure 3 for the step with $a = 1$ and $b = 2$. Immediately, we recognise that there are at least three regions of interest: (i) both turning points on the solid boundary for $0 < A < 1$; (ii) one point on the surface and one on the solid boundary for $1 < A < (b/a)^2$; and both points back on the solid boundary for $A > (b/a)^2$.

In addition to these three regions, we must also note the positions of the Stokes lines relative to the turning points. It will be useful to introduce labels by

- C : Capillary Stokes line from stagnation point, $\zeta = -b$
- G : Gravity Stokes line from corner point, $\zeta = -a$
- \overline{T}_1 and \underline{T}_1 : Capillary/gravity Stokes line from first turning point, $\zeta = \zeta_1$
- T_2 : Capillary/gravity Stokes line from second turning point, $\zeta = \zeta_2$

The underline, \underline{T}_1 , is used to distinguish when the first turning point lies on bottom boundary and the overline, \overline{T}_1 , for when it lies on the free-surface.

Next, examine the six subplots on the right of Figure 4, corresponding to six regions

labelled **1** and **6**. These subplots indicate the qualitative arrangement of the turning points and Stokes lines for various values of $A > 0$. Solution-types are then classified by a sequence of labels, indicating the events as we traverse the free-surface from left to right (in the downstream direction). For example, a sequence like

$$\underline{T}_1 \cdot T_2 \cdot C \cdot G$$

in Region 1 corresponds to traversing the free-surface in the downstream direction, and crossing (i) the \underline{T}_1 Stokes line, (ii) the T_2 Stokes line, (iii) the capillary Stokes line from the stagnation point, and (iv) the gravity Stokes line from the corner.

Similarly, a sequence like

$$C \cdot \overline{T}_1 \cdot G$$

in Region 4 corresponds to (i) crossing the C -line, (ii) crossing the \overline{T}_1 point on the free-surface, and then (iii) crossing the G -line.

The sequence of subfigures in the right of Figure 4 thus indicates that in the low-Froude, low-Bond limit, there are six possible solution types. Examine now the $\beta\tau$ -plane shown in the left frame of Figure 4. The extremum cases of **1** and **6** correspond to the standard linearised solutions of Part 1 and confirms that the gray region of Figure 3, which corresponds to $1 < A < (b/a)^2$, is further subdivided into **2** to **5**. Thus, this figure shows that the usual dispersion ‘line’ which differentiates Rayleigh’s two scenarios actually contains a *series* of solutions **2** to **5**; the line’s thickness and these new solutions are a manifestation of the nonlinearity (and largeness) of the step. As the step-height tends to zero, the line thickness tends to zero and we recover the standard linear picture.

Remember that the physical sketches on the right subplots of Figure 4 are only illustrative projections of the Stokes lines from the upper half- ζ -plane onto the physical domain (see Figure 2 of Part 1). The reader should not forget that in crossing a Stokes line along the free surface, a wave contribution due to the singularities in the lower half- ζ -plane also switch on; indeed the sum of these two contributions was used to derive (4.8).

In the following discussion, it is sufficient to only consider the wave contributions from the upper half- ζ -plane. We shorten the notation for the arguments of the exponentials in (4.7b) and (6.13) by expressing the integrals relative to either the stagnation point, $\zeta = -a$, or the corner point, $\zeta = -b$. Thus

$$X_{\text{cap}} = -\frac{1}{\epsilon} \int_{-a}^{\zeta} \frac{d\chi_-}{d\zeta'} d\zeta' \quad \text{and} \quad X_{\text{grav}} = -\frac{1}{\epsilon} \int_{-b}^{\zeta} \frac{d\chi_+}{d\zeta'} d\zeta'. \quad (7.2)$$

We also denote the pre-factors for the exponentials by a calligraphic letter with a subscript, if applicable, which corresponds to an interaction with a turning point. This leads to the three symbols:

- \mathcal{A} : An arbitrary wave amplitude to be determined
- \mathcal{C} : A capillary wave amplitude generated from the stagnation point
- \mathcal{G} : A gravity wave amplitude generated from the corner point.

Here are three examples:

$$(i) \mathcal{G} e^{X_{\text{grav}}} \quad (ii) \mathcal{A}_{\overline{T}_1 T_2} e^{X_{\text{cap}}} \quad (iii) (\mathcal{A} + \mathcal{C})_{\overline{T}_1} e^{X_{\text{grav}}}$$

Example (i) denotes a gravity wave with amplitude \mathcal{G} switched on after crossing the Stokes line from the corner. Example (ii) is constructed in a two-step process: an (arbitrary) capillary wave with amplitude \mathcal{A} encounters a turning point and switches on a gravity wave with amplitude $\mathcal{A}_{\overline{T}_1}$, then encounters the second turning point and switches on a

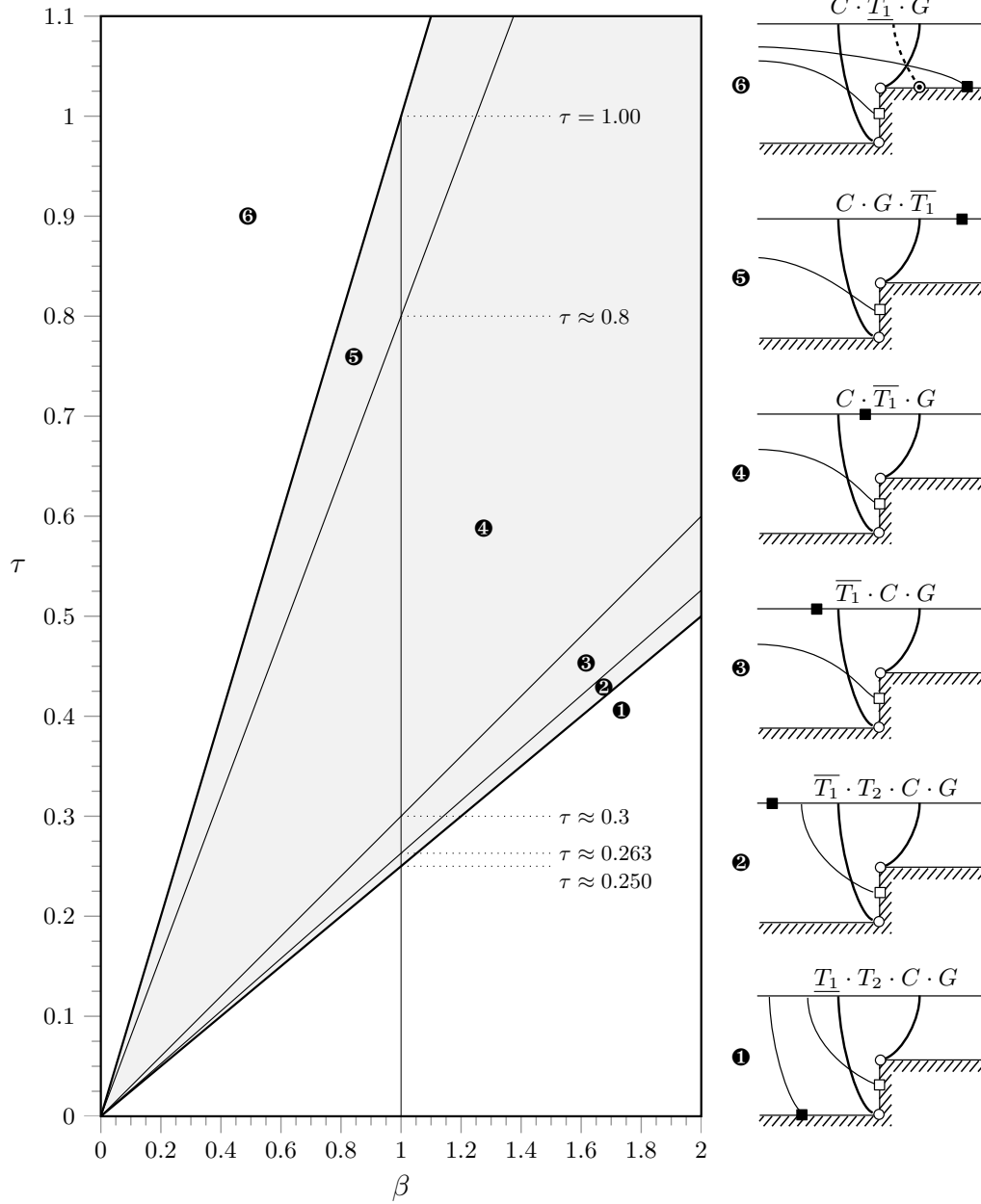


FIGURE 4. The six regimes of interest for flow over a rectangular step, as shown in the $\beta\tau$ -plane (left) for the case of $a = 1$ and $b = 2$. The gray strip is bounded by $A = 1$ and $A = (b/a)^2$, which thickens for larger and larger steps. The arrangement of Stokes lines and turning points is shown on the right. Stagnation and corner points are circular nodes and turning points are square nodes. The arrangement in Region 6 is complicated and will be discussed in §7.6.

capillary wave with amplitude $\mathcal{A}_{\overline{T_1 T_2}}$. Example (iii) is constructed by beginning with a capillary wave with combined pre-factors \mathcal{A} and \mathcal{C} (the former an arbitrary quantity, and the latter generated from the stagnation point), and then switching on a gravity wave due to the $\overline{T_1}$ turning point. Our notation and the associated expressions will be made clear in the many examples and figures to follow.

7.1. Region 1 with $\overline{T_1} \cdot T_2 \cdot C \cdot G$

Consider the case of $A < 1$. For most (larger) values of τ , as we analytically continue across the free-surface, the sequence of events is $\overline{T_1} \cdot T_2 \cdot C \cdot G$, which involves the T_2 Stokes line crossing the C Stokes line. In fact, for extremely small values of τ , the lines may not actually cross, and so the sequence is $\overline{T_1} \cdot C \cdot T_2 \cdot G$; however, both cases are equivalent because, as we shall see, the turning points do not play any role in determining the free surface.

In order to derive the correct wave expressions, we traverse the free-surface, from left-to-right, beginning with a wave that satisfies the upstream radiation condition (*i.e.* a capillary wave). Upon reaching the end, we apply the downstream radiation condition, and this process provides us with a complete set of fully-determined waves. If we start with an arbitrary upstream capillary wave $\mathcal{A}e^{X_{\text{cap}}}$, then the sequence of events is

$$\begin{aligned} \mathcal{A}e^{X_{\text{cap}}} &\xrightarrow[\textcircled{\text{G}} > \textcircled{\text{C}}]{\overline{T_1}} \mathcal{A}e^{X_{\text{cap}}} \\ &\xrightarrow[\textcircled{\text{G}} > \textcircled{\text{C}}]{T_2} \mathcal{A}e^{X_{\text{cap}}} \\ &\xrightarrow[\textcircled{\text{B}} > \textcircled{\text{C}}]{\text{Stag.}} (\mathcal{A} + \mathcal{C})e^{X_{\text{cap}}} \\ &\xrightarrow[\textcircled{\text{B}} > \textcircled{\text{G}}]{\text{Corn.}} (\mathcal{A} + \mathcal{C})e^{X_{\text{cap}}} + \mathcal{G}e^{X_{\text{grav}}}. \end{aligned}$$

There are no capillary waves downstream, so $\mathcal{A} + \mathcal{C} = 0$, and the final solution has

$$-\mathcal{C}e^{X_{\text{cap}}} \xrightarrow[\textcircled{\text{B}} > \textcircled{\text{C}}]{\text{Stag.}} 0 \xrightarrow[\textcircled{\text{B}} > \textcircled{\text{G}}]{\text{Corn.}} \mathcal{G}e^{X_{\text{grav}}},$$

where the pre-factors, \mathcal{C} and \mathcal{G} , are given by the jump condition (4.7b), with

$$\mathcal{C} = -\frac{2\pi i Q_+}{\epsilon^{\gamma_C}} \quad \text{and} \quad \mathcal{G} = -\frac{2\pi i Q_-}{\epsilon^{\gamma_G}} \quad (7.3)$$

and Q_{\pm} is computed from (3.14) and (3.15). For the rectangular step, it can be shown by matching inner and outer solutions that $\gamma_C = 0$ and $\gamma_G = 6/5$. In the end, the free-surface resembles the standard linearised solution with capillary waves upstream and gravity waves downstream, but now, with a wave-free region near the centre, similar to what occurs in Part 1 of our work. The result is sketched in Figure 5(a). Note that the Stokes lines from the turning points remain inactive.

In some problems, the intersection of Stokes lines can lead to more subtle effects, such as the higher-order Stokes Phenomenon (see for example, Howls *et al.* 2004). A simple consistency check is to analytically continue in a closed path around the intersection point, and to see if the solution returns to its original value. In this case, we see that the T_2 Stokes line remains inactive, and so the intersection of the $\textcircled{\text{B}} > \textcircled{\text{C}}$ and $\textcircled{\text{G}} > \textcircled{\text{C}}$ lines are not a concern. This will not be the case for the solution in Region 6.

7.2. Region 2 with $\overline{\overline{T_1}} \cdot T_2 \cdot C \cdot G$

As τ is increased and β held steady, the $\overline{\overline{T_1}}$ turning point moves upstream along the solid boundary and reaches $-\infty$ at $A = 1$. Solutions in Region 2 have $A > 1$ and the

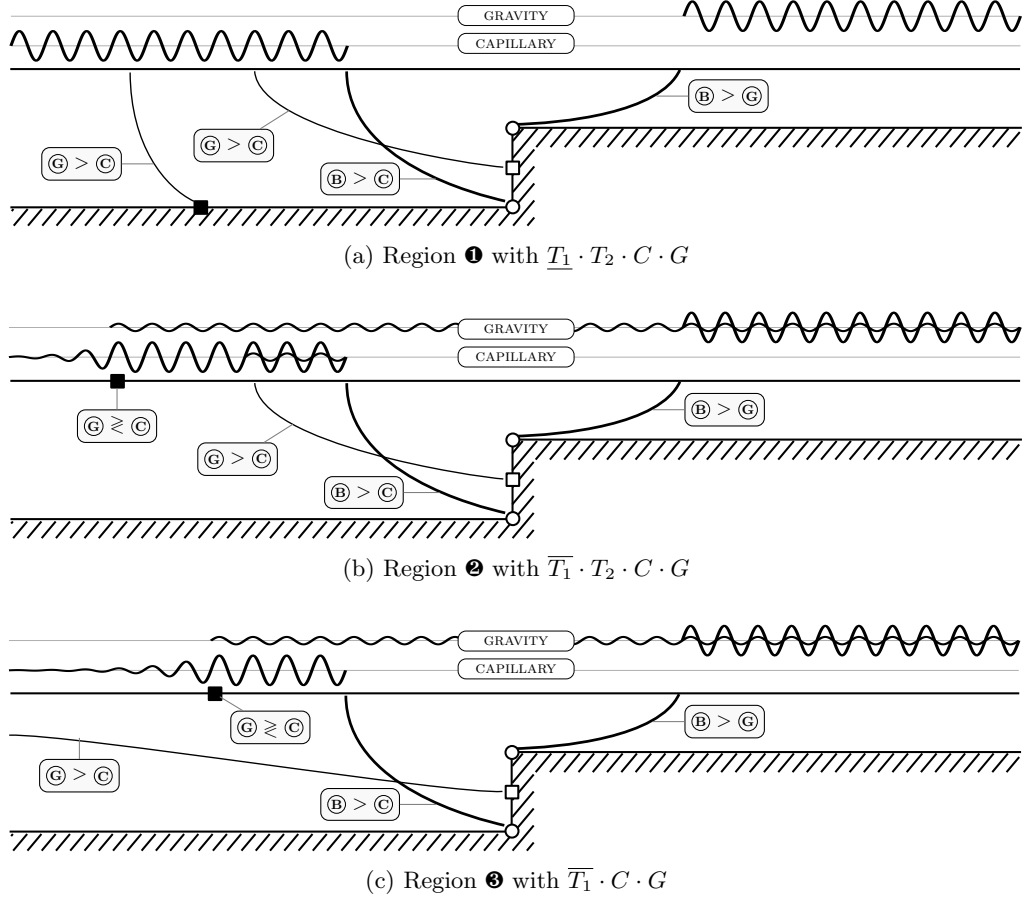


FIGURE 5. Sketch of gravity-capillary solutions in Regions ❶ to ❸. Waves sketched with the larger amplitudes are switched on by the stagnation point or corner; waves sketched with smaller amplitudes are switched on by turning points. Note that the gravity and capillary waves differ in both amplitude and wavelength, but we have not illustrated this difference.

turning point \overline{T}_1 has now moved onto the free-surface and travels downstream as τ is further increased. The turning point on the free-surface also implies that upstream waves will now decay, but downstream waves will remain constant. We start with an arbitrary upstream capillary wave $\mathcal{A}e^{X_{\text{cap}}}$, and the sequence of events is:

$$\begin{aligned}
 \mathcal{A}e^{X_{\text{cap}}} &\xrightarrow{\substack{\overline{T}_1 \\ \textcircled{G} \geq \textcircled{C}}} \mathcal{A}e^{X_{\text{cap}}} + \mathcal{A}_{\overline{T}_1}e^{X_{\text{grav}}} \\
 &\xrightarrow{\substack{T_2 \\ \textcircled{G} > \textcircled{C}}} (\mathcal{A} + \mathcal{A}_{\overline{T}_1 T_2})e^{X_{\text{cap}}} + \mathcal{A}_{\overline{T}_1}e^{X_{\text{grav}}} \\
 &\xrightarrow{\substack{\text{Stag.} \\ \textcircled{B} > \textcircled{C}}} (\mathcal{A} + \mathcal{A}_{\overline{T}_1 T_2} + \mathcal{C})e^{X_{\text{cap}}} + \mathcal{A}_{\overline{T}_1}e^{X_{\text{grav}}} \\
 &\xrightarrow{\substack{\text{Corn.} \\ \textcircled{B} > \textcircled{G}}} (\mathcal{A} + \mathcal{A}_{\overline{T}_1 T_2} + \mathcal{C})e^{X_{\text{cap}}} + (\mathcal{A}_{\overline{T}_1} + \mathcal{G})e^{X_{\text{grav}}}.
 \end{aligned}$$

The last transition is known by (4.7b), so \mathcal{G} is again given by (7.3). Since there are no capillary waves downstream, and \mathcal{C} is provided by the jump condition in (4.7b), then

$$\mathcal{C} = -\mathcal{A} - \mathcal{A}_{\overline{T}_1 T_2} = -\frac{2\pi i Q_+}{\epsilon^{\gamma C}}. \quad (7.4)$$

We can associate the pre-factor \mathcal{A} with the stagnation point, writing

$$\mathcal{A}(\zeta) = \left[-\frac{2\pi i Q_{\pm}}{\epsilon^{\gamma c}} \right] \widehat{\mathcal{A}}(\zeta), \quad (7.5)$$

for some unknown function, $\widehat{\mathcal{A}}(\zeta)$. The pre-factor, $\mathcal{A}_{\overline{T}_1}$, of the first gravity wave switched on by the \overline{T}_1 turning-point is given by the transition rule (6.13), and this allows us to relate $\widehat{\mathcal{A}}$ to $\mathcal{A}_{\overline{T}_1}$. Care must be taken to express the gravitational wave quantities with respect to the corner, instead of the stagnation point [see the definition of X_{grav} in (7.2)]. Next, the pre-factor, $\mathcal{A}_{\overline{T}_1 T_2}$, of the second capillary wave switched on by the T_2 turning point is also given by (6.13), which relates $\widehat{\mathcal{A}}$ to $\mathcal{A}_{\overline{T}_1 T_2}$. Lastly, (7.4) and (7.5) allows \mathcal{A} to be solved entirely in terms of Q_{\pm} and thus all quantities can be determined.

Therefore, far upstream we have a decaying capillary wave, while far downstream we have a constant gravity wave. Also, switched on after encountering the \overline{T}_1 turning point is a (doubly) exponentially small gravity wave, which continues downstream. Finally, there is an even smaller capillary wave which has been turned on by the gravity wave across the T_2 -line. This is illustrated in Figure 5(b), and in summary,

$$\begin{aligned} \mathcal{A}e^{X_{\text{cap}}} \xrightarrow[\textcircled{\mathbb{C}} \geq \textcircled{\mathbb{C}}]{\overline{T}_1} \mathcal{A}e^{X_{\text{cap}}} + \mathcal{A}_{\overline{T}_1}e^{X_{\text{grav}}} \xrightarrow[\textcircled{\mathbb{C}} > \textcircled{\mathbb{C}}]{T_2} (\mathcal{A} + \mathcal{A}_{\overline{T}_1 T_2})e^{X_{\text{cap}}} + \mathcal{A}_{\overline{T}_1}e^{X_{\text{grav}}} \\ \xrightarrow[\textcircled{\mathbb{B}} > \textcircled{\mathbb{C}}]{\text{Stag.}} \mathcal{A}_{\overline{T}_1}e^{X_{\text{grav}}} \xrightarrow[\textcircled{\mathbb{B}} > \textcircled{\mathbb{C}}]{\text{Corn.}} (\mathcal{A}_{\overline{T}_1} + \mathcal{G})e^{X_{\text{grav}}}. \end{aligned} \quad (7.6)$$

In contrast to Region 1, the T_2 line is now active, but the intersection of the two Stokes lines remains unproblematic; we can still analytically continue in a closed path around the intersection point and return to our original value.

We note that the solutions in this region are actually contained in a rather small section of $\beta\tau$ -space (as shown in Figure 4). Once \overline{T}_1 has crossed the point that marks the intersection of the T_2 line and the free-surface, a bifurcation occurs and the T_2 line tends to $w = -\infty$ without intersecting the free-surface; this can be verified by numerical integration.

7.3. Region 3 with $\overline{T}_1 \cdot C \cdot G$

In Region 3, the only difference to the previous region is that the T_2 -line tends to $w = -\infty$ without intersecting the free surface. Starting with an arbitrary upstream capillary wave, $\mathcal{A}e^{X_{\text{cap}}}$, the sequence of events is now:

$$\begin{aligned} \mathcal{A}e^{X_{\text{cap}}} \xrightarrow[\textcircled{\mathbb{C}} \geq \textcircled{\mathbb{C}}]{\overline{T}_1} \mathcal{A}e^{X_{\text{cap}}} + \mathcal{A}_{\overline{T}_1}e^{X_{\text{grav}}} \\ \xrightarrow[\textcircled{\mathbb{B}} > \textcircled{\mathbb{C}}]{\text{Stag.}} (\mathcal{A} + \mathcal{C})e^{X_{\text{cap}}} + \mathcal{A}_{\overline{T}_1}e^{X_{\text{grav}}} \\ \xrightarrow[\textcircled{\mathbb{B}} > \textcircled{\mathbb{C}}]{\text{Corn.}} (\mathcal{A} + \mathcal{C})e^{X_{\text{cap}}} + (\mathcal{A}_{\overline{T}_1} + \mathcal{G})e^{X_{\text{grav}}}. \end{aligned}$$

The downstream radiation condition requires $\mathcal{C} = -\mathcal{A}$. Like the previous regions, (7.3) provides the expressions for \mathcal{C} and \mathcal{G} , and (6.13) relates \mathcal{A} to $\mathcal{A}_{\overline{T}_1}$. The final result is

$$\begin{aligned} \mathcal{A}e^{X_{\text{cap}}} \xrightarrow[\textcircled{\mathbb{C}} \geq \textcircled{\mathbb{C}}]{\overline{T}_1} \mathcal{A}e^{X_{\text{cap}}} + \mathcal{A}_{\overline{T}_1}e^{X_{\text{grav}}} \\ \xrightarrow[\textcircled{\mathbb{B}} > \textcircled{\mathbb{C}}]{\text{Stag.}} \mathcal{A}_{\overline{T}_1}e^{X_{\text{grav}}} \xrightarrow[\textcircled{\mathbb{B}} > \textcircled{\mathbb{C}}]{\text{Corn.}} (\mathcal{A}_{\overline{T}_1} + \mathcal{G})e^{X_{\text{grav}}}. \end{aligned}$$

Thus the only difference between the solutions in Regions 2 and 3 is that in the latter,

the doubly-exponentially-small capillary wave has disappeared from the free surface. A sketch of the solution is shown in Figure 5(c).

7.4. Region 4 with $C \cdot \overline{T_1} \cdot G$

For A still larger, $\overline{T_1}$ eventually crosses the intersection point of the C -line and the free-surface, and then the sequence is then $C \cdot \overline{T_1} \cdot G$. If we start with an arbitrary upstream capillary wave $\mathcal{A}e^{X_{\text{cap}}}$, the sequence of events is

$$\begin{aligned} \mathcal{A}e^{X_{\text{cap}}} &\xrightarrow[\mathbb{B} > \mathbb{C}]{\text{Stag.}} (\mathcal{A} + \mathcal{C})e^{X_{\text{cap}}} \\ &\xrightarrow[\mathbb{C} \geq \mathbb{C}]{\overline{T_1}} (\mathcal{A} + \mathcal{C})e^{X_{\text{cap}}} + (\mathcal{A} + \mathcal{C})_{\overline{T_1}}e^{X_{\text{grav}}} \\ &\xrightarrow[\mathbb{B} > \mathbb{C}]{\text{Corn.}} (\mathcal{A} + \mathcal{C})e^{X_{\text{cap}}} + ((\mathcal{A} + \mathcal{C})_{\overline{T_1}} + \mathcal{G})e^{X_{\text{grav}}}. \end{aligned}$$

Again, we cannot have capillary waves downstream, so $\mathcal{A} + \mathcal{C} = 0$, and the coefficients, \mathcal{C} and \mathcal{G} , are given by (7.3). The final result is

$$-\mathcal{C}e^{X_{\text{cap}}} \xrightarrow[\mathbb{B} > \mathbb{C}]{\text{Stag.}} 0 \xrightarrow[\mathbb{B} > \mathbb{C}]{\text{Corn.}} \mathcal{G}e^{X_{\text{grav}}}.$$

The solution is sketched in Figure 6(a), and we see that it consists of a decaying capillary wave upstream and a constant amplitude gravity wave downstream.

7.5. Region 5 with $C \cdot G \cdot \overline{T_1}$

Eventually, $\overline{T_1}$ passes the point where the G -line intersects the free-surface, and so downstream from this point, the gravity waves switch from constant-amplitude to exponentially decaying oscillations. For solutions in this region, it is easier to analytically continue from downstream to upstream, and negate each of the transitions [since the rules (4.7b) and (6.13) are written for continuation in the downstream direction]. If we start with an arbitrary downstream gravity wave $\mathcal{A}e^{X_{\text{grav}}}$, the sequence follows

$$\begin{aligned} \mathcal{A}e^{X_{\text{grav}}} &\xleftarrow[\mathbb{C} \geq \mathbb{C}]{\overline{T_1}} -\mathcal{A}_{\overline{T_1}}e^{X_{\text{cap}}} + \mathcal{A}e^{X_{\text{grav}}} \\ &\xleftarrow[\mathbb{B} > \mathbb{C}]{\text{Corn.}} -\mathcal{A}_{\overline{T_1}}e^{X_{\text{cap}}} + (\mathcal{A} - \mathcal{G})e^{X_{\text{grav}}} \\ &\xleftarrow[\mathbb{B} > \mathbb{C}]{\text{Stag.}} (-\mathcal{A}_{\overline{T_1}} - \mathcal{C})e^{X_{\text{cap}}} + (\mathcal{A} - \mathcal{G})e^{X_{\text{grav}}}. \end{aligned}$$

We impose the requirement that there are no gravity waves downstream, so $\mathcal{A} - \mathcal{G} = 0$. The values \mathcal{B}_S and \mathcal{C}_C are given in (7.3), and \mathcal{A} and $\mathcal{A}_{\overline{T_1}}$ are related through (6.13). The final result is given by (from left to right)

$$(-\mathcal{A}_{\overline{T_1}} - \mathcal{C})e^{X_{\text{cap}}} \xrightarrow[\mathbb{B} > \mathbb{C}]{\text{Stag.}} -\mathcal{A}_{\overline{T_1}}e^{X_{\text{cap}}} \xrightarrow[\mathbb{B} > \mathbb{C}]{\text{Corn.}} -\mathcal{A}_{\overline{T_1}}e^{X_{\text{cap}}} + \mathcal{A}e^{X_{\text{grav}}} \xrightarrow[\mathbb{C} \geq \mathbb{C}]{\overline{T_1}} \mathcal{A}e^{X_{\text{grav}}}.$$

The solution is shown in Figure 6(b), where we see it consists of two decaying capillary waves upstream, and a gravity wave downstream. The gravity wave, which is first switched on by the Stokes line from the corner, decays until it reaches the turning point, and then switches to a constant amplitude wave downstream.

7.6. Region 6 with $C \cdot G$

Once $A = (b/a)^{1/2}$, the $\overline{T_1}$ point has reached $w = \infty$ and for larger values of A , the turning point begins to move from right-to-left along the downstream solid boundary.

There is one issue which needs to be addressed: in Figure 6(c), the $\mathbb{B} > \mathbb{C}$ line intersects the $\mathbb{C} > \mathbb{C}$ line at a *Stokes Crossing Point* or SCP. If we analytically continue

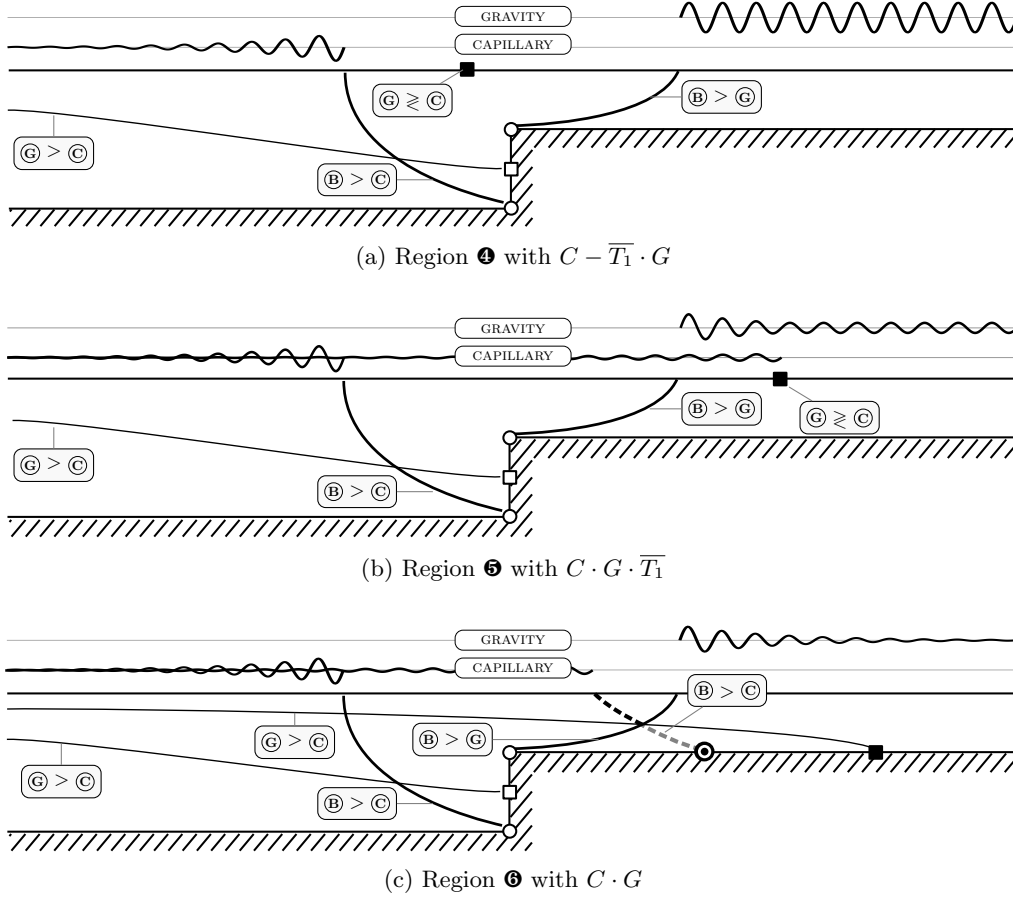


FIGURE 6. Sketch of gravity-capillary solutions in Regions 4 to 6. The solution in Region 6 should correspond to the second of Rayleigh’s linearised profiles, but is complicated by the two crossing Stokes lines. In Appendix A, we demonstrate the existence of a third Stokes line (dashed), which originates from a secondary singularity (black circle).

in a path that encircles the SCP, then we find that in order to avoid an inconsistency, the base solution must switch-off a capillary wave somewhere along the path; in other words, there must be a $\textcircled{B} > \textcircled{C}$ line, which goes through the SCP. However, neither the corner, nor the stagnation point, produces such a Stokes line.

This issue is addressed in Appendix A, where we discuss three key ideas: (i) there is a second singularity [marked by the black circle in Figure 6(c)]. This singularity does not appear in any of the early terms (3.2a)–(3.2d), but represents a singularity in the late terms of the late terms. It lies on the adjacent Riemann sheet from the originally defined corner point, $\zeta = a$, and can be detected by setting $\chi = 0$, where from (3.8)

$$\chi = -i \int_{\Gamma} \left[\frac{q_0^2 - \sqrt{\Delta}}{2\tau q_0} \right] d\varphi.$$

The contour Γ begins at $\zeta = a$, crosses the branch cut from the turning point, \bar{T}_1 , and continues along the secondary Riemann sheet of $\sqrt{\Delta}$.

In the appendix, we also establish that (ii) the secondary singularity produces a $\textcircled{B} > \textcircled{C}$ Stokes line that crosses the SCP [shown dashed in Figure 6(c)]. Finally, (iii) the portion of

the $\textcircled{B} > \textcircled{C}$ line that joins the SCP to the singularity must be inactive; this switching-off of a Stokes line is due to the higher-order Stokes Phenomenon. These more complicated issues of secondary singularities, Stokes crossing points, and the higher-order Stokes Phenomenon, have been studied by others in a variety of different situations [see for example Berk *et al.* (1982); Howls *et al.* (2004); Olde Daalhuis (2004); Chapman *et al.* (1999); Chapman & Mortimer (2005); Chapman *et al.* (2007)].

The solution is then

$$\left(-\mathcal{C} + \mathcal{G}_{T_1}\right) e^{X_{\text{cap}}} \xrightarrow[\textcircled{B} > \textcircled{C}]{\text{Stag.}} \mathcal{G}_{T_1} e^{X_{\text{cap}}} \xrightarrow[\textcircled{B} > \textcircled{C}]{\text{Sec. Sing.}} 0 \xrightarrow[\textcircled{B} > \textcircled{C}]{\text{Corn.}} \mathcal{G} e^{X_{\text{grav}}},$$

where the values of \mathcal{C} and \mathcal{G} are given by (7.3). The pre-factor \mathcal{G}_{T_1} reminds us that the capillary wave is switched-on by taking the \mathcal{G} gravity wave and crossing the Stokes line from the the turning point; its value can be computed from (6.13). These doubly exponentially small capillary waves are switched off downstream upon crossing the Stokes line from the secondary singularity.

Decaying waves on either side of the step are exactly what we expect from the linear analysis; however, we see that the result is not quite the same as in the linearised theory due to the presence of the doubly-small capillary waves upstream. The free surface is shown in Figure 6(c). However, we note that, as for the case of pure gravity waves (see Chapman & Vanden-Broeck 2006), we would expect a distinguished limit in the small Froude, small Bond, and small step height limits. Thus relating the results here with the work in Part 1 is not likely to be a trivial problem.

8. Discussion

Now having reached the end of our work on the gravity-capillary problem, we have one final query: *do these new waves truly exist?*

Our theoretical predictions form the first attempt of exploring the previously unknown region of low-Froude and low-Bond numbers. Our results posit the existence of six different families of waves for flow over a step (**1** to **6** in Figure 4), and reveals that the usual dispersion curve separating linear solutions **1** and **6** widens if we include the nonlinear nature of the geometry. While this structure is only valid at low Froude and low Bond numbers, it also sheds new light on the general complexity of gravity-capillary problem, which has been freely acknowledged in the past.

Many open questions remain, some of which may ultimately hold the key to detecting these new waves (or discounting their existence). Throughout this work, we have provided a clear analysis of the *local* issues of the gravity-capillary problem. For example, we have shown how the emergence of a Stokes line depends on the local angle of the obstruction, or how the switching-on of waves near turning points can be predicted via an Airy-like transition. Although we have not shown the tedious calculations, the crucial pre-factor, Λ , is another local issue, and can be derived by matching inner and outer solutions near the singularities (see Trinh 2010 for more details). But what about the *global* properties of the Stokes lines?

For example, can a Stokes line emerge from a singularity along a secondary Riemann sheet, only to later return to the primary sheet and intersect the free surface? Our analysis in Appendix A attempted to answer this question by drawing a comparison to a similar problem containing multiple singularities and crossing Stokes lines; we then used these results to propose the likely free-surface configuration for the complicated situation of Region 6 of Figure 6(c). However, a more rigorous treatment of these issues remains an open problem.

Equally fascinating is the myriad of configurations that now seems possible for free-surface gravity-capillary flows over different geometries. A classic question is to inquire whether there are special geometries for which leading-order wave cancellation occurs and where, for example, the waves produced by one singularity cancels the waves produced by another. Although these issues regarding variable geometries have been studied in the context of pure gravity or capillary waves (Chapman & Vanden-Broeck 2002; Trinh *et al.* 2011; Lustri *et al.* 2012; Trinh & Chapman 2013*a*), a catalogue of the wave configurations for different geometries in the combined gravity-capillary case is a subject of future work.

Finally, the most significant question is why have these waves not been previously detected? From the perspective of numerical simulations, one plausible difficulty concerns the so-called *radiation problem*: it is unclear how the upstream radiation condition can be accurately implemented in a numerical scheme. This difficulty is highlighted in, for example, the works of Forbes (1983), Scullen (1998), and Grandison & Vanden-Broeck (2006). For gravity-capillary flow past a large obstruction, the resultant solutions are influenced by the chosen treatment of the far field, and it is possible that inherent errors in current numerical methods make it difficult to differentiate between the structure of our new gravity-capillary waves and the typical linearised solutions. Do these waves truly exist? Our theoretical results suggest that they do; the search for such configurations, either in nature or in the digital world, forms the basis of ongoing investigation.

Appendix A. On the crossing of Stokes lines

We address the issue of the crossing of Stokes lines in the gravity-capillary problem by drawing an analogy to the same phenomenon which occurs in a modified Airy equation:

$$\epsilon^2 y'' = xy + \frac{e^{x/\epsilon}}{x-a}.$$

This equation was chosen because it not only possesses an (Airy) turning point at $x = 0$, but also an additional singularity at $x = a$. Writing $y = ve^{x/\epsilon}$ gives

$$\epsilon^2 v'' + 2\epsilon v' + (1-x)v = \frac{1}{x-a}, \quad (\text{A } 1)$$

where we also require $v \rightarrow 0$ as $|x| \rightarrow \infty$. We can now perform the standard asymptotic analysis of (A 1), expanding $v = \sum \epsilon^n v_n$, and giving the first two orders as

$$v_0 = \frac{1}{(1-x)(x-a)} \quad (\text{A } 2)$$

$$v_1 = \frac{-2}{(a-x)^3(x-a)} + \frac{2}{(1-x)^2(x-a)^2}, \quad (\text{A } 3)$$

and in general, for $n \geq 2$,

$$v_n = -\frac{1}{1-x} \left[v''_{n-2} + 2v'_{n-1} \right]. \quad (\text{A } 4)$$

As $n \rightarrow \infty$, we expect the singularities at $x = 0$ and $x = a$ to produce factorial over power divergence of the late terms. Substituting the ansatz

$$v_n \sim \frac{V(x)\Gamma(n+\gamma)}{[\chi(x)]^{n+\gamma}},$$

into (A 4) gives $(\chi')^2 - 2\chi' + (1 - x) = 0$, or solving yields

$$\chi = \int^x 1 \pm s^{1/2} ds. \quad (\text{A } 5)$$

There are clearly singularities at $x = 1$ and $x = a$, and we shall focus on the exponentials generated by the latter. At a Stokes line emerging from the singularity at $x = a$, the base series can switch-on exponentials of the form, $e^{-\chi/\epsilon}$ with χ being one of

$$\chi_1 = x + \frac{2}{3}x^{3/2} - a - \frac{2}{3}a^{3/2} \quad (\text{A } 6)$$

$$\chi_2 = x - \frac{2}{3}x^{3/2} - a + \frac{2}{3}a^{3/2}. \quad (\text{A } 7)$$

If we use $\textcircled{\text{B}}$ to denote the base series, and $\textcircled{1}$ and $\textcircled{2}$ for the two exponentials, then the Stokes Phenomenon describes the process in which $\textcircled{\text{B}} > \textcircled{1}$ or $\textcircled{\text{B}} > \textcircled{2}$. However, there is also a turning point at $x = 0$, for which the associated Stokes lines can cause interactions between the two exponentials. If $\textcircled{1} > \textcircled{2}$, then this produces an exponential with

$$\chi_3 = x - \frac{2}{3}x^{3/2} - a - \frac{2}{3}a^{3/2}, \quad (\text{A } 8)$$

since the Airy transition simply requires switching the branch of $x^{3/2}$. Similarly, if $\textcircled{2} > \textcircled{1}$, this produces an exponential with

$$\chi_4 = x + \frac{2}{3}x^{3/2} - a + \frac{2}{3}a^{3/2}. \quad (\text{A } 9)$$

The Stokes lines for the case $a = -1 + i$ are shown in the left frame of Figure 7. Notice that the $\textcircled{\text{B}} > \textcircled{1}$ Stokes line intersects the $\textcircled{1} > \textcircled{2}$ line at a Stokes Crossing Point (SCP). If we analytically continue in a circle around the SCP, we see that a third Stokes line, with $\textcircled{\text{B}} > \textcircled{2}$, is needed in order to avoid an inconsistency. From (A 8), this seems to require a singularity at the point $x = x_*$, where $\chi_3 = 0$; for $a = -1 + i$, the singularity lies at $x_* \approx -1.423 - 0.509i$. There is a similar singularity at $x \approx 0.249 + 0.883i$, where $\chi_4 = 0$, which we associate with a $\textcircled{\text{B}} > \textcircled{1}$ line. The curiosity, however, is that these singularities do not appear anywhere in the base series, $\textcircled{\text{B}}$, and so they do not seem to be associated with any eventual divergence.

To explore this in more detail, we define the Fourier transform as

$$\widehat{v}(k) = \frac{1}{\sqrt{2\pi}} \int_{-\infty}^{\infty} v(x) e^{ikx} dx,$$

and take the transform of (A 1), giving

$$i\epsilon^2 k^2 \widehat{v} - 2\epsilon k \widehat{v} - i\widehat{v} + \frac{d\widehat{v}}{dk} = \sqrt{2\pi} e^{iak} H(k),$$

where $H(k)$ is the Heaviside function, and we have assumed that $\Im(a) > 0$. Solving this equation yields

$$\widehat{v} = \sqrt{2\pi} \exp \left[\frac{i\epsilon^2 k^3}{3} + \epsilon k^2 + ik \right] \int_0^k \exp \left[\frac{i\epsilon^2 u^3}{3} - \epsilon u^2 - iu + iau \right] du,$$

or once inverted,

$$v = \int_{-\infty}^{\infty} \exp \left[\frac{i\epsilon^2 k^3}{3} + \epsilon k^2 + ik - ikx \right] \int_0^k \exp \left[\frac{i\epsilon^2 u^3}{3} - \epsilon u^2 - iu + iau \right] du dk.$$

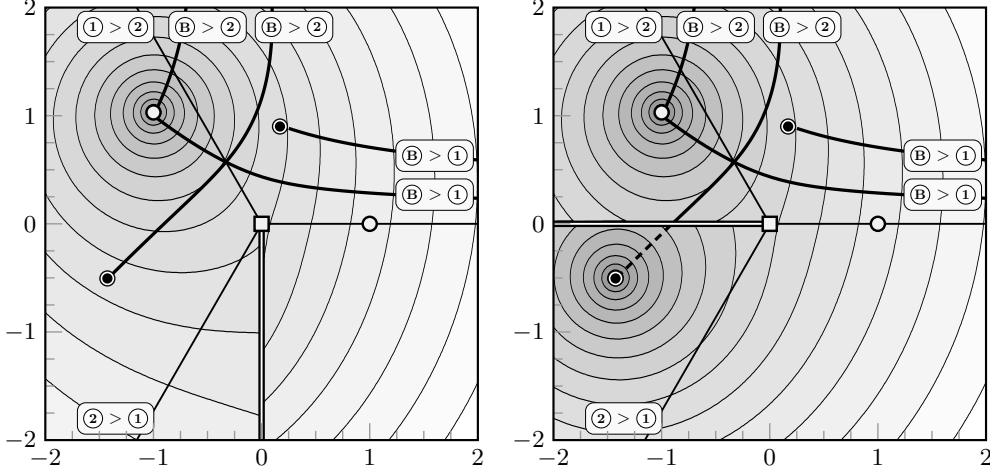


FIGURE 7. Stokes lines in the complex x -plane, shown with two different choices of branch cuts (left/right). White circles denote the singularities at $x = a$ and $x = 1$, black circles are the secondary singularities, and a square denotes the turning point. The Stokes lines from $x = 1$ are not drawn. Branch cuts are shown as a striped line, and the dashed lines are used to indicate points on a secondary Riemann sheet. Background contours are for $|\chi_3|$ (left) or $|\chi_1|$ (right), with darker regions indicating smaller values.

We rescale $k = s/\epsilon$ and $i = v/\epsilon$, giving

$$v = \int_{-\infty}^{\infty} \exp\left[-\frac{\phi(s; x)}{\epsilon}\right] \int_0^s \exp\left[\frac{\phi(v; a)}{\epsilon}\right] dv ds, \quad (\text{A } 10)$$

where we have defined

$$\phi(v; a) = \frac{iv^3}{3} - v^2 - iv + aiv.$$

In the limit $\epsilon \rightarrow 0$, the dominant contributions of the innermost integral in (A 10) come from the end points at $v = 0$ and $v = s$, or at the two saddle points at $v = -i \pm i\sqrt{a}$. Thus (A 10) can be approximated as a sum of integrals of the form

$$\int_{-\infty}^{\infty} A(s) e^{\psi(s)/\epsilon} ds, \quad (\text{A } 11)$$

where ψ is one of

$$\psi(s) = \begin{cases} is(a-x) & (\text{A } 12) \\ -\frac{is^3}{3} + s^2 + is - isx & (\text{A } 13) \\ -\frac{is^3}{3} + s^2 + is - isx - \frac{1}{3} + a \pm \frac{2a^{3/2}}{3} & (\text{A } 14) \end{cases}$$

Approximating the integral (A 11) using (A 12) recovers the base series (A 2)–(A 3). The second and third expressions for ψ have saddle points at $s = -i \pm i\sqrt{x}$. Using the second expression (A 13), we see that the integral (A 11) produces contributions $e^{-\chi/\epsilon}$ with

$$\chi = -\frac{1}{3} + x \pm \frac{2}{3}x^{3/2}.$$

One of these comes from the singularity at $x = 1$; the other comes from the same singularity, and then going around the turning point.

Finally, approximating the integral at the saddle points using the third expression for ψ in (A 14), gives four possible expressions for χ . Two of these are directly from the singularity at $x = a$, and return χ_1 and χ_2 from (A 6)–(A 7). The other two, returning χ_3 and χ_4 in (A 8)–(A 9), are generated by the same singularity, but involve an integration contour which goes around the turning point. This verifies that the missing Stokes line should be there, though it does not shed much light on the mysterious singularity, $x = x_*$.

Let us go back to the expansion. We can write the n^{th} term, v_n , from (A 4) as

$$v_n = \sum_{k=1}^{n+1} \sum_{m=0}^{2n} \frac{a_{k,m}}{(x-a)^k (1-x)^m}, \quad (\text{A } 15)$$

with $a_{k,m}$ given by

$$\begin{aligned} a_{k,m} = & 2(k-1)a_{k-1,m-1} - 2(m-2)a_{k,m-2} - (k-2)a_{k-2,m-1} - (k-2)^2 a_{k-2,m-1} \\ & + 2(k-1)(m-2)a_{k-1,m-2} - (m-3)a_{k,m-3} - (m-3)^2 a_{k,m-3}. \end{aligned}$$

We believe that if this recurrence relation is solved, and the method of steepest descents is used to approximate the terms (A 15) as $n \rightarrow \infty$, then the mysterious point, $x = x_*$, would appear as a singularity in the late terms of the late terms, v_n . These ‘secondary’ singularities and SCPs have been encountered in Chapman & Mortimer (2005) and Howls *et al.* (2004).

Before moving to the gravity-capillary problem, we clarify a labelling issue: the prescription of x_* by $\chi_3 = 0$ in (A 8) is correct only if the $\textcircled{\text{B}} > \textcircled{\text{2}}$ Stokes line can be continued from the SCP to the secondary singularity, x_* , along the same branch of $x^{3/2}$ (as it is drawn in the left frame of Figure 7). However, a different choice of the branch cut (as in the right frame) shows that $\chi_1 = 0$ is the correct equation. To correct this ambiguity, we use an alternative notation. Let $x_{(k)}$ correspond to a point on the k^{th} Riemann sheet (associated with the two branches of $x^{3/2}$); that is, $x_{(k)}$ is mapped to $e^{\pi ik} x^{3/2}$, with $k = 0, 1$. From (A 5), we then write χ_1 as

$$\chi_1 = \int_{a_{(0)}}^x \left[1 + e^{\pi ik(s)} s^{3/2} \right] ds, \quad (\text{A } 16)$$

where $k(s) = 0$ or 1 , depending on which sheet the integrand is currently on. This makes it very clear that the secondary singularity, x_* , is still given by $\chi_1 = 0$, but x_* may either lie on the sheet with $a_{(0)}$, or the sheet with $a_{(1)}$. Thus, χ_3 in (A 8) is simply

$$\chi_3 = \left(\int_{a_{(0)}}^{a_{(1)}} + \int_{a_{(1)}}^x \right) \left[1 + e^{\pi ik(s)} s^{3/2} \right] ds,$$

except that x is restricted to the same sheet as $a_{(1)}$, since (A 8) requires principal branches taken throughout. Writing χ_1 in the form (A 16) serves to emphasize the fact that the contribution χ_3 is found by beginning at $a_{(0)}$ and then crossing onto the secondary sheet.

A.1. Crossing Stokes lines in the gravity-capillary problem

We now address the issue of the crossing Stokes lines in Region 6 of §7.6. For χ in (3.10), there are three types of branch points, but only the ones from the turning points are relevant. Remembering that the corner of the step is at $\zeta = a$, and changing to integration in ζ using (2.4), we denote, for the gravity wave,

$$\chi_g = i \int_{a_{(1)}}^{\zeta} \left[\frac{q_0^2 + e^{\pi ik(s)} \sqrt{\Delta}}{2\tau q_0} \right] \frac{1}{s} ds, \quad (\text{A } 17)$$

where $k(s) = 1$ on the branch of $a_{(1)}$ and $k(s) = 0$ on the branch of $a_{(0)}$ (associated with the capillary wave). In addition to the two turning points, there is a logarithmic branch point from the factor of s^{-1} , and two square-root branch points from the two singularities of q_0 . The former type adds a constant to χ upon crossing the cut, while latter type switches q_0 to $-q_0$ upon crossing the cut. If we wanted to fully explore the different sheets, it would be better to write $\zeta = \zeta_{(k_1, k_2, k_3, k_4, k_5)}$, to keep track of how many times we have gone around each of the five branch points. However for our purpose, only the single turning point which causes the intersection is important.

Remember: the issue is that the crossing of the $\textcircled{B} > \textcircled{C}$ and $\textcircled{C} > \textcircled{C}$ lines in Figure 6(c) also requires a $\textcircled{B} > \textcircled{C}$ line in order to avoid an inconsistency. Like the example of the preceding section, this missing Stokes line comes from a secondary singularity, $\zeta = \zeta^\bullet$, not present in any of the early orders. To see this, we write (A 17) in the form

$$\chi_g = i \left(\int_{a_{(1)}}^{a_{(0)}} + \int_{a_{(0)}}^{\zeta} \right) \left[\frac{q_0^2 + e^{\pi i k(s)} \sqrt{\Delta}}{2\tau q_0} \right] \frac{1}{s} ds, \quad (\text{A } 18)$$

and we further restrict ζ to the $k = 0^{\text{th}}$ Riemann sheet. Thus, (A 18) is an integral from $a_{(1)}$ to $a_{(0)}$ via the branch cut from the turning point, and then proceeds from $a_{(0)}$ to ζ . The second integral is the usual capillary integral (hence the capillary wave). This new representation is used to make Figure 8; the most important feature of the figure is the missing singularity and its missing Stokes line, which indeed intersects the SCP.

In addition to the appearance of the secondary singularity, intersecting Stokes lines are typically accompanied by yet another subtlety: that of the Higher-Order Stokes Phenomenon [see again Howls *et al.* (2004) and Chapman & Mortimer (2005)]. This phenomenon specifies that at a SCP, Stokes lines may themselves switch-off. Indeed, this must be the case because if we analytically continue around the SCP in the inset of Figure 6(c), we see that both portions of the $\textcircled{B} > \textcircled{C}$ line (on either side of the SCP) can not be active. It remains to determine whether the portion of the Stokes line connecting the singularity to the SCP is active, or whether it is rather the portion from the SCP to the free surface.

To address this issue, we note in Figure 8 that if the dashed Stokes line is followed from the SCP to the secondary singularity into the lower half-plane, then it changes from a $\textcircled{B} > \textcircled{C}$ Stokes line to a $\textcircled{B} > \textcircled{C}$ Stokes line across the secondary singularity ($\zeta = \zeta^\bullet$). In fact, the portion of the axis where $-b \leq \zeta \leq \zeta_1$, corresponds to the Anti-Stokes lines (where $\textcircled{B} = \textcircled{C} = \textcircled{C}$) from the corner ($\zeta = -b$) and turning point ($\zeta = \zeta_1$). Across the secondary singularity, then, the Stokes line has changed character abruptly, and we argue by analogy to studies of the Higher-Order Stokes Phenomenon that this can not occur unless ζ^\bullet is a turning point (which it is not). Thus, the portion of the Stokes lines connected to the secondary singularity is inactive. Finally, we add that in Figure 8, the dashed Stokes line is the only line associated with secondary Riemann sheets that we have chosen to show. There are other Stokes lines we have not shown (and in fact, other secondary singularities), but these are not relevant to the free surface waves.

REFERENCES

- BENDER, C. M. & ORSZAG, S. A. 1978 *Advanced Mathematical Methods for Scientists and Engineers*. McGraw-Hill, Inc.
- BERK, H. L., NEVINS, W. M. & ROBERTS, K. V. 1982 New Stokes' line in WKB theory. *J. Math. Phys.* **23** (6), 988–1002.
- BERRY, M. V. 1989 Uniform asymptotic smoothing of Stokes discontinuities. *Proc. Roy. Soc. London A* **422**, 7–21.

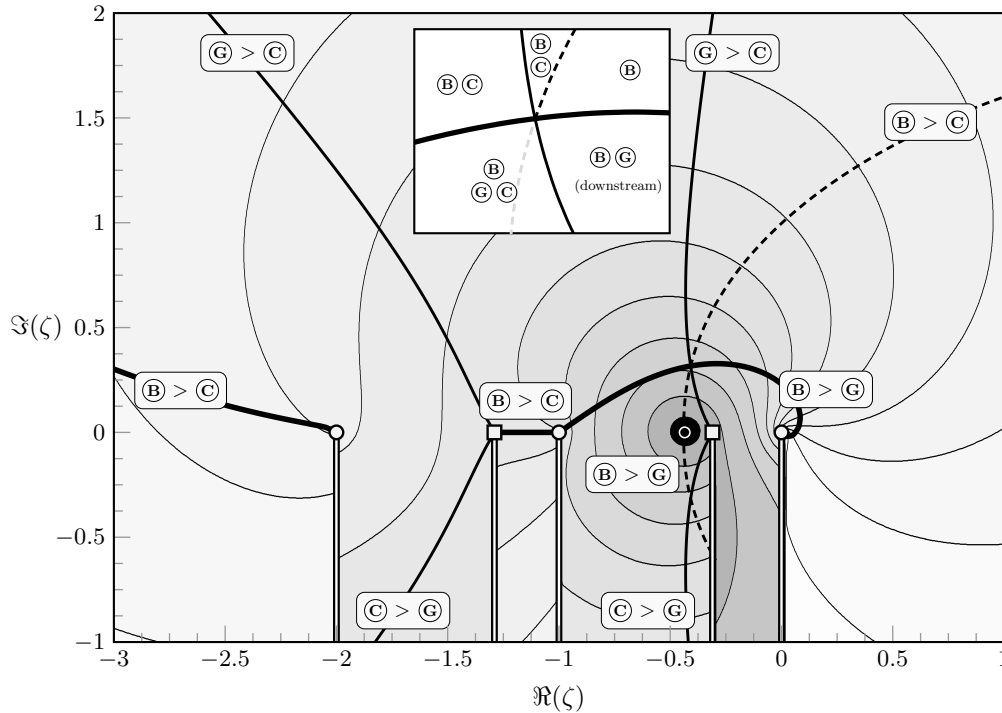


FIGURE 8. The underlying contours and shading represent $|\chi_g|$ from (A 18), with dark regions indicating small values. Values of $\beta = 1$ and $\tau = 1.5$ were used, and $a = 1$, $b = 2$ for the corner and stagnation points (circles). Turning points are $\zeta_1 \approx -0.310$ and $\zeta_2 \approx -1.290$ (squares), and the Stokes lines were computed using (5.1) and (6.4). Note that with the exception of the Stokes line from ζ_2 , all the Stokes lines that begin in the upper-half plane will eventually intersect $\zeta \in \mathbb{R}^+$. Branch cuts are shown striped. The secondary singularity, located at $\zeta^\bullet \approx -0.435$, is shown as a black circle, and its Stokes line shown dashed (note that this Stokes line, as well as the singularity, lies on a different Riemann sheet than the other components of the figure). The inset confirms that if we analytically continue around the SCP, beginning with the base solution upstream, then a portion of the new Stokes line must switch off across the SCP (gray, dashed).

- BOYD, J. P. 1998 *Weakly nonlocal solitary waves and beyond-all-orders asymptotics*. Kluwer Academic Publishers.
- CHAPMAN, S. J., HOWLS, C. J., KING, J. R. & OLDE DAALHUIS, A. B. 2007 Why is a shock not a caustic? The higher-order Stokes phenomenon and smoothed shock formation. *Nonlinearity* **20** (10), 2425.
- CHAPMAN, S. J., KING, J. R. & ADAMS, K. L. 1998 Exponential asymptotics and Stokes lines in nonlinear ordinary differential equations. *Proc. R. Soc. Lond. A* **454**, 2733–2755.
- CHAPMAN, S. J., LAWRY, J. M. H., OCKENDON, J. R. & TEW, R. H. 1999 On the theory of complex rays. *SIAM Rev.* **41** (3), 417–509.
- CHAPMAN, S. J. & MORTIMER, D. B. 2005 Exponential asymptotics and Stokes lines in a partial differential equation. *Proc. R. Soc. A* **461** (2060), 2385–2421.
- CHAPMAN, S. J. & VANDEN-BROECK, J.-M. 2002 Exponential asymptotics and capillary waves. *SIAM J. Appl. Math.* **62** (6), 1872–1898.
- CHAPMAN, S. J. & VANDEN-BROECK, J.-M. 2006 Exponential asymptotics and gravity waves. *J. Fluid Mech.* **567**, 299–326.
- COSTIN, O. 2008 *Asymptotics and Borel summability*, vol. 141. Chapman & Hall/CRC.
- DIAS, F. & KHARIF, C. 1999 Nonlinear gravity and capillary-gravity waves. *Ann. Rev. Fluid Mech.* **31** (1), 301–346.

- DINGLE, R. B. 1973 *Asymptotic Expansions: Their Derivation and Interpretation*. Academic Press, London.
- FORBES, L. K. 1983 Free-surface flow over a semi-circular obstruction, including the influence of gravity and surface tension. *J. Fluid Mech.* **127**, 283–297.
- GRANDISON, S. & VANDEN-BROECK, J.-M. 2006 Truncation approximations for gravity-capillary free-surface flows. *J. Eng. Math.* **54**, 89–97.
- HOWLS, C. J., LANGMAN, P. J. & DAALHUIS, A. B. OLDE 2004 On the higher-order Stokes Phenomenon. *Proc. R. Soc. Lond. A* **460**, 2285–2303.
- KING, A. C. & BLOOR, M. I. G. 1987 Free-surface flow over a step. *J. Fluid. Mech.* **182**, 193–208.
- LAMB, H. 1932 *Hydrodynamics*. Dover Publications.
- LUSTRI, C. J., MCCUE, S. W. & BINDER, B. J. 2012 Free surface flow past topography: A beyond-all-orders approach. *Eur. J. Appl. Math.* **1** (1), 1–27.
- LUSTRI, C. J., MCCUE, S. W. & CHAPMAN, S. J. 2013 Exponential asymptotics of free surface flow due to a line source. *IMA J. Applied Math.* (Submitted) .
- OLDE DAALHUIS, A. B. 2004 On higher-order Stokes phenomena of an inhomogeneous linear ordinary differential equation. *J. Comput. Appl. Math.* **169**, 235–246.
- LORD RAYLEIGH 1883 The form of standing waves on the surface of running water. *Proc. Lond. Math. Soc.* **15**, 69–78.
- SCULLEN, D. C. 1998 Accurate computation of steady nonlinear free-surface flows. PhD thesis, University of Adelaide.
- STOKER, J. J. 1957 *Water waves*. Interscience Publishers, Inc.
- TRINH, P. H. 2010 Exponential asymptotics and free-surface flows. PhD thesis, University of Oxford.
- TRINH, P. H. & CHAPMAN, S. J. 2013a Do waveless ships exist? Part II: The multi-cornered hull. *Submitted to J. Fluid Mech.* .
- TRINH, P. H. & CHAPMAN, S. J. 2013b New theoretical gravity-capillary waves. Part 1: Linear theory. *Submitted to J. Fluid Mech.* .
- TRINH, P. H., CHAPMAN, S. J. & VANDEN-BROECK, J.-M. 2011 Do waveless ships exist? Results for single-cornered hulls. *J. Fluid Mech.* **685**, 413–439.
- VANDEN-BROECK, J.-M. 2010 *Gravity-Capillary Free-Surface Flows*. Cambridge, UK: Cambridge University Press.
- WHITE, R. B. 2005 *Asymptotic Analysis of Differential Equations*. Imperial College Press.